

**Charles University
Faculty of Medicine in Hradec Králové**

Doctoral degree programme
Clinical Biochemistry

**Epigenetic Regulation of Adhesive Molecules in High-grade
Serous Ovarian Carcinoma**

**Epigenetická regulace adhezivních molekul u high-grade
serózního ovariálního karcinomu**

Ivana Baranová, M.Sc.

Supervisor: Prof. Vladimír Palička, M.D., Ph.D.
Consultant supervisor: Marcela Chmelařová, M.Sc., Ph.D.

Hradec Králové, 2019

Author's Declaration

Declaration:

I declare hereby that this dissertation thesis is my own original work and that I indicated by references all used information sources. I also agree with depositing my dissertation in the Medical Library of the Charles University, Faculty of Medicine in Hradec Králové and with making use of it for study and educational purpose provided that anyone who will use it for his/her publication or lectures is obliged to refer to or cite my work properly.

I give my consent to availability of my dissertation's electronic version in the information system of the Charles University.

Hradec Králové, 2019

Signature of the author

Acknowledgments

I would like to express my sincere gratitude to my supervisor Prof. Vladimír Palička, M.D., Ph.D., for his continuous support of my doctoral study and related research, for his guidance, encouragement and words of motivation.

This dissertation would not have been possible without the help and support of my consultant supervisor Marcela Chmelařová, M.Sc., Ph.D., who shared her experiences and provided constructive and valuable advices from the very beginning of my study.

I would also like to thank Assoc. prof. Iva Sedláková, M.D., Ph.D. from Department of Obstetrics and Gynecology, and Prof. Jan Laco, M.D., Ph.D., from The Fingerland Department of Pathology, for their help with collecting samples and collaboration on research projects.

My sincere thanks go to my colleagues from Department of Molecular Biology, Institute of Clinical Biochemistry and Diagnostics, especially Helena Kovaříková, M.Sc., Veronika Hyršlová, M.Sc., Albína Přikrylová, and Natálie Birknerová. Their support and friendly approach made the hard work little bit easier.

The research was supported by the Ministry of Health – conceptual development of research organization (UHHK, 00179906), by the Ministry of Education, Youth and Sports (PROGRES Q40/11 and SVV 260398), and by the project BBMRI_CZ LM2015089.

Table of Contents

Summary CZE	7
Summary ENG.....	8
List of Figures	9
List of Tables.....	10
Abbreviations	11
1 Introduction.....	12
1.1 Ovarian cancer	12
1.1.1 Epidemiology	12
1.1.2 Etiopathogenesis.....	14
1.1.3 Symptoms, diagnosis and treatment.....	16
1.1.4 Epithelial-mesenchymal transition in ovarian cancer	18
1.1.5 High-grade serous ovarian carcinoma.....	19
1.2 Epigenetics in ovarian cancer	20
1.2.1 DNA methylation	20
1.2.2 Posttranscriptional regulation by microRNA	25
1.2.3 Histone modifications	27
1.2.4 Epigenetic therapy of ovarian cancer.....	28
1.3 Adhesion molecules.....	29
2 Objectives.....	32
3 Materials and Methods	33
3.1 Study group.....	33
3.2 DNA extraction.....	34
3.3 Bisulfite conversion of DNA.....	35
3.4 Next-generation sequencing	36
3.5 Real-time PCR-based methods for detecting DNA methylation.....	43
3.5.1 Methylation sensitive high-resolution melting analysis	43
3.5.2 Real-time methylation specific analysis.....	45
3.6 The Cancer Genome Atlas methylation data.....	47
3.7 Statistical analysis.....	47
4 Results	49
4.1 Next-generation sequencing	49

4.1.1	Cadherins.....	50
4.1.2	Protocadherins.....	51
4.1.3	Catenins.....	53
4.2	Confirmation methods.....	53
4.2.1	<i>CDH13</i> methylation.....	53
4.2.2	<i>PCDH17</i> methylation.....	54
4.3	TCGA methylation data analysis.....	55
4.3.1	<i>CDH13</i> methylation.....	55
4.3.2	<i>PCDH7</i> methylation.....	55
4.4	Follow-up.....	56
4.5	DNA methylation panel.....	58
5	Discussion.....	60
6	Conclusions.....	68
	References.....	70
	Appendices.....	80
	A1 FIGO staging classification for cancer of the ovary, fallopian tube, and peritoneum.....	80
	A2 Methylation of catenins detected by next-generation sequencing.....	81
	A3 Follow-up data of patients and methylation status of analyzed genes.....	84
	A4 Methylation analysis of <i>HNF1B</i> and <i>GATA4</i> genes.....	86

Summary CZE

Nedostatek účinných biomarkerů pro screening a včasnou detekci ovariálního karcinomu je v současné době považován za jeden z nejnaléhavějších problémů onkogynekologie. Vzhledem k tomu, že k epigenetickým změnám dochází již v počátcích karcinogeneze, mohly by být tyto změny využity jako screeningové markery u rizikové populace. Epigenetické mechanismy se mimo jiné podílejí i na regulaci adhezivních molekul, které sehrávají důležitou roli při rozvoji nádoru a tvorbě metastáz.

Hlavním cílem této práce byla analýza změn v metylaci u vybraných kadherinů a kateninů v ovariální nádorové tkáni v porovnání s kontrolní tkání. Vyšetřovaný soubor tvořilo 68 pacientek s high-grade serózním ovariálním karcinomem (HGSOK) a 46 kontrolních pacientek. Pro stanovení oblastí s nejvýznamnějšími změnami v metylaci ve vybraných genech bylo využito masivně paralelního sekvenování. Pro potvrzení metylačních změn v místech s největším potenciálem byla použita metylačně-senzitivní vysokorozlišovací analýza křivek tání a metylačně-specifická kvantitativní polymerázová řetězová reakce. Dalším cílem práce bylo vytvoření panelu biomarkerů, který by mohl být v budoucnu využit při screeningu HGSOK. Vybrané kadheriny byly proto hodnoceny společně s transkripčními faktory, u kterých byla nalezena hypermetylace již v naší předchozí studii.

Významné změny v metylaci u nádorových vzorků byly odhaleny zejména v genech kódujících *CDH13* a *PCDH17*, přičemž metylace v kontrolních vzorcích nebyla pozorována. Při společné analýze obou genů byla metylace detekována u 65,6 % nádorových vzorků. Vytvořením panelu 4 genů, který kromě *CDH13* a *PCDH17* obsahoval také *HNF1B* a *GATA4*, bylo dosaženo senzitivity 88,5 % při 100%-ní specificitě a efektivitě 93,3 %.

Naše výsledky svědčí o tom, že metylace genů *CDH13* a *PCDH17* by mohla hrát důležitou roli při vzniku a rozvoji HGSOK. Jejich potenciál je patrný zejména po zahrnutí do širšího panelu biomarkerů. K potvrzení těchto nových výsledků jsou však zapotřebí další studie na rozsáhlejší souboru pacientů.

Summary ENG

The lack of effective biomarkers for screening and early detection of ovarian cancer is currently considered as one of the most pressing problems in oncogynecology. Because epigenetic alterations occur early in the cancer development, they provide great potential to serve as such biomarkers. Epigenetic mechanisms have been implicated also in regulation of adhesion molecules that play a major role in cancer progression.

The main aim of this study was to investigate the methylation pattern of selected cadherin and catenin genes in ovarian cancer tissue by comparison with control tissue. The study group consisted of 68 patients with high-grade serous ovarian cancer (HGSOC) and 46 control patients. To determine the sites with the most significant methylation in selected genes next-generation sequencing was employed. For further confirmation of detected methylation of selected regions, methylation-sensitive high-resolution melting analysis and real-time methylation-specific polymerase chain reaction were used. In attempt to design potential biomarker panel for future screening of HGSOC as the secondary aim of our study, cadherins were evaluated together with transcription factors from our previous study.

Significant methylation-positive pattern was detected in *CDH13* and *PCDH17* genes. Simultaneous analysis of both genes together revealed methylation in 65.6 % of tumor samples, whereas control samples were methylation free. Four-gene methylation panel, that beside *CDH13* and *PCDH17* included also *HNF1B* and *GATA4* genes, reached sensitivity of 88.5 % with 100% specificity and 93.3% efficiency.

Our results indicate that methylation of the *CDH13* and *PCDH17* genes could play an important role in development and progression of HGSOC. With the right selection of the most relevant sites for methylation analysis these genes showed potential to become a target in search for new epigenetic biomarkers, especially as a part of a biomarker panel. However, further studies on more extensive group of patients are needed to confirm these novel results.

List of Figures

Figure 1 Time trend of crude incidence and mortality for ovarian carcinoma in the Czech Republic.

Figure 2 Age structure of patients diagnosed with ovarian carcinoma in the Czech Republic.

Figure 3 Schematic representation of DNA methylation.

Figure 4 Major families of cell adhesion molecules.

Figure 5 Distribution of tumor stages in study group.

Figure 6 Age distribution of study group.

Figure 7 Schematic illustration of bisulfite conversion.

Figure 8 Schematic representation of PCR-based methods used for DNA methylation analysis.

Figure 9 Next-generation sequencing workflow.

Figure 10 *CTNND2* sequencing run data from BaseSpace Sequence Hub.

Figure 11 Next-generation sequencing methylation data of cadherins.

Figure 12 Next-generation sequencing methylation data of protocadherins.

Figure 13 High-resolution melting analysis of *CDH13_a* amplicon.

Figure 14 Kaplan-Meier survival curves according to the methylation of *CDH13* gene.

Figure 15 Kaplan-Meier survival curves according to the methylation of *PCDH17* gene.

Figure A2.1 Next-generation sequencing methylation data of *CTNNA2*.

Figure A2.2 Next-generation sequencing methylation data of *CTNND2*, short amplicon.

Figure A2.3 Next-generation sequencing methylation data of *CTNND2*, long amplicon.

Figure A4.1 Next-generation sequencing methylation data of *GATA4* and *HNF1B*.

List of Tables

Table 1 Clinical and molecular characteristics of the epithelial ovarian cancer subtypes

Table 2 Deregulated miRNAs detected in ovarian tissue associated with diagnosis of various types of ovarian cancer

Table 3 Deregulated miRNAs detected in blood associated with diagnosis of various types of ovarian cancer

Table 4 Amplicon characteristics and primer sequences in next-generation sequencing

Table 5 PCR protocol for first round amplification using AmpliTaq Gold DNA Polymerase

Table 6 PCR protocol for first round amplification using Platinum *Taq* DNA Polymerase

Table 7 PCR protocol for first round amplification of CTNNA2_2 using High Fidelity Platinum *Taq* DNA Polymerase

Table 8 Amplicon characteristics and primer sequences used in MS-HRM analysis

Table 9 Protocol for MS-HRM analysis of *CDH13* amplicons and *PCDH17*

Table 10 PCR protocol for real-time methylation analysis of *CDH13* gene

Table 11 Diagnostic parameters of analyzed genes included in DNA methylation panel

Table A1.1 FIGO staging classification for cancer of the ovary, fallopian tube, and peritoneum

Table A3.1 Follow-up data of patients and methylation status of analyzed genes

Table A4.1 Amplicon characteristics and primer sequences used for next-generation sequencing of *GATA4* and *HNF1B*

Table A4.2 PCR protocol for methylation specific analysis of *GATA4*

Table A4.3 Protocol for MS-HRM analysis of *HNF1B*

Abbreviations

BC DNA	Bisulfite Converted DNA
bp	Base Pair
CAM	Cell Adhesion Molecule
CpG	Cytosine-phosphate-Guanine
DNMT	DNA Methyltransferase
dNTPs	Deoxynucleotide Triphosphates
DFS	Disease-Free Survival
EMT	Epithelial-Mesenchymal Transition
EOC	Epithelial Ovarian Cancer
FFPE	Formalin-Fixed, Paraffin-Embedded
FN	False Negatives
FP	False Positives
FT	Fallopian Tube
HDAC	Histone Deacetylase
HGSOC	High-Grade Serous Ovarian Carcinoma
HRM	High-Resolution Melting
miRNA	Micro RNA
MS-HRM	Methylation Sensitive High-Resolution Melting
NGS	Next-Generation Sequencing
NPV	Negative Predictive Value
OC	Ovarian Cancer
OS	Overall Survival
PCR	Polymerase Chain Reaction
PPV	Positive Predictive Value
TCGA	The Cancer Genome Atlas
TP	True Positives
TN	True Negatives
WHO	World Health Organization

Because of the common use of gene symbols, they are not included in the list of abbreviations.

1 Introduction

1.1 Ovarian cancer

Ovarian cancer (OC) is currently considered to be one of the most pressing problems in oncogynecology. Vague early symptoms that lead to diagnosis at advanced stages, in addition to the lack of effective screening test, and often aggressive nature of the disease predestinate OC to be the most fatal cancer of female reproductive system.

1.1.1 Epidemiology

Worldwide, OC has the 7th worst mortality rate of all female cancers. In 2018, there were estimated 295,414 new cases of OC, giving an incidence rate of 6.6/100,000 women, and 184,799 deaths, giving a mortality rate of 3.9/100,000 women (Ferlay et al., 2018). Incidence and mortality rates vary according to a country; in general, they are higher in more developed countries. In the Czech Republic, 1,012 new cases of OC were diagnosed in 2018, giving an incidence rate of 9.5/100,000 and 827 women died due OC, giving a mortality rate of 6.7/100,000 (International Agency for Research on Cancer, 2019). All rates were calculated as the age-standardized rates (ASR). The standardization takes into account influence of age as a significant factor in the risk of cancer when comparing several populations with different age structure.

Recently, there has been some mild decrease in the incidence of OC, which is probably caused by more precise modern histopathological diagnostics (e.g. metastatic colorectal carcinoma was often misclassified as OC) and change in epidemiology factors, such as widespread use of hormonal contraceptives. Also, mortality rates have leveled or even declined over past decades. But again, there are substantial differences in OC patterns and trends across world regions. Figure 1 shows time trend of crude incidence and mortality in the Czech Republic between years 1977–2016 (Dušek et al., 2005). However, the Globocan study estimates that by 2040, there will be worldwide increase in incidence by 47 % to 434,184 cases a year and deaths will increase by 58.6 % to 293,039. Estimation for the Czech Republic predicts annual increase

in incidence by 12 % to 1,133 new cases of OC and deaths will increase to 982 (18.7 %). (International Agency for Research on Cancer, 2019)

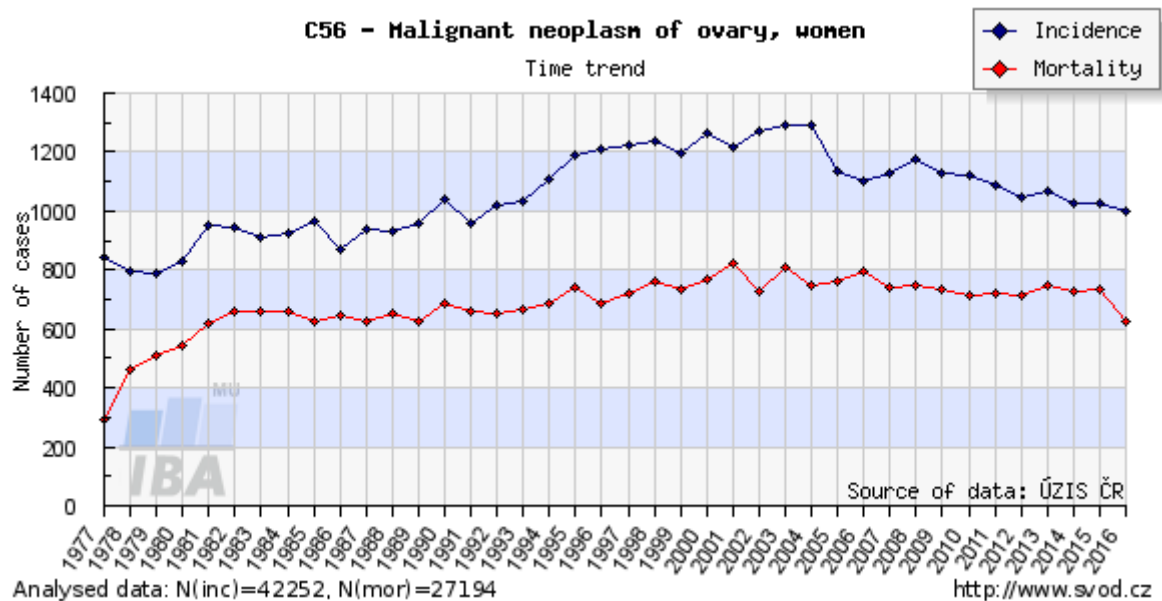


Figure 1 Time trend of crude incidence and mortality for ovarian carcinoma in the Czech Republic (downloaded from Dušek et al., 2005).

Like incidence and mortality rates also survival rates in OC vary widely across the world. The current five-year survival rates range between 30 % and 50 %, and in general have begun to improve over the last 20 years (Bhatla et Jones, 2018).

According to the CONCORD-3 study, in the Czech Republic, there were 18,875 cases of OC diagnosed between years 2000–2014. Estimated five-year survival for the women diagnosed in 2005–2009 is 35.2 %, for those diagnosed in 2010–2014 the estimation increased to 36.5 %. (Allemani et al., 2018)

The median age at diagnosis of OC is 63 years. Figure 2 displays an age structure of patients diagnosed with OC in the Czech Republic between years 1977–2016 (Dušek et al., 2005). *BRCA* mutation carriers have a lower median age at diagnosis; they may be a decade younger than patients without *BRCA* mutations. Germline mutations of *BRCA1* and *BRCA2* genes are present in approximately 12–14 % of patients with OC, the highest rate occur in HGSOC (~ 18 %) (Weiderpass et Tyczynski, 2015). Somatic *BRCA* mutations have been found in approximately 5–7 % of OC patients. Overall, *BRCA1/2* mutations are found in approximately 20 % of all OC cases (Moschetta et al., 2016).

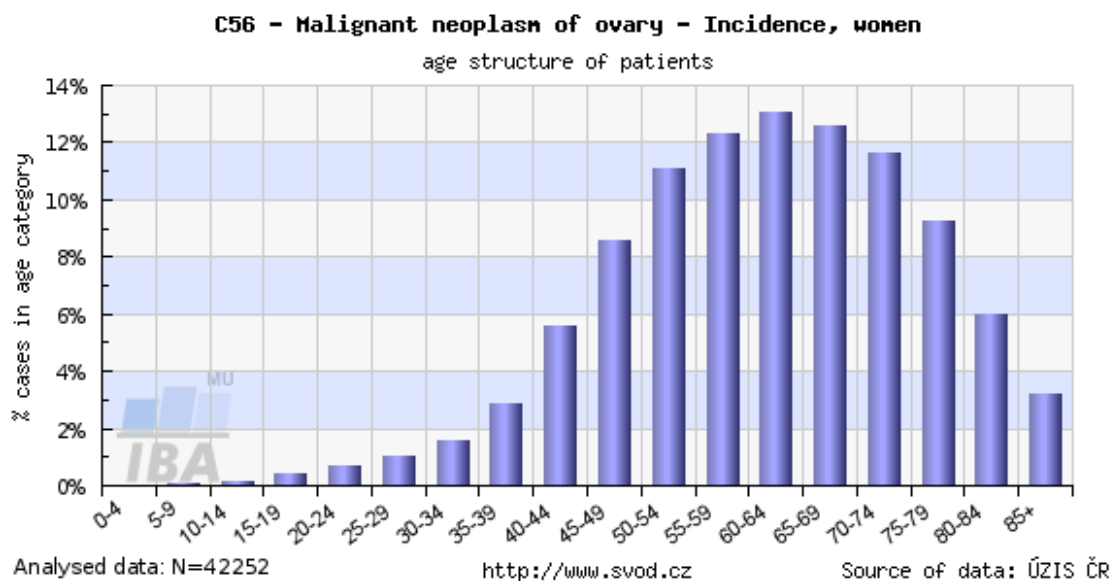


Figure 2 Age structure of patients diagnosed with ovarian carcinoma in the Czech Republic (downloaded from Dušek et al., 2005).

The estimated prevalence of *BRCA* mutations in general population is very low (0.1–0.25 %). However, it may vary considerably in different geographical regions and ethnic groups. The higher frequency has been described in the population of Central and Eastern Europe, Iceland, Netherlands, Sweden, Norway, Germany, France, Spain and especially among Ashkenazi Jews (Balmana et al., 2009). The individuals of Ashkenazi Jewish descent carry the *BRCA* mutations ten times more frequently than the rest of population; the estimated prevalence is 2.5 % (Manchanda et al., 2015).

1.1.2 Etiopathogenesis

OC is a nonspecific term for any cancerous growth that occurs in the ovary and covers heterogeneous group of tumors with distinct morphologic, prognostic, etiopathogenetic, and molecular characteristics. According to the 2014 World Health Organization (WHO) classification of tumors of female reproductive organs approximately 10 % of all OC are non-epithelial malignancies comprising of germ cell tumors (e.g. dysgerminomas, choriocarcinoma, immature teratomas) and sex-cord stromal tumors (e.g. granulosa cell tumors, fibromas) (Kurman et al, 2014). However, the majority of OC are classified as epithelial ovarian cancer (EOC).

Based on series of histomorphological, immunohistochemical and molecular-genetic analyzes, EOC was divided into five major subtypes: high-grade serous, endometrioid, clear cell, low-grade serous, and mucinous (Kurman et al., 2014).

As indicated by differences in genetic risk factors, precursor lesions, response to chemotherapy, prognosis, and molecular abnormalities, these types are essentially distinct diseases (Prat, 2012). Main characteristics of EOC subtypes are summarized in Table 1.

Table 1 Clinical and molecular characteristics of the epithelial ovarian cancer subtypes (adapted from Prat, 2012)

Type	HGSC	EC	CCC	MC	LGSC
Percentage of all OC	70	10	10	3	<5
Genetic risk factors	<i>BRCA1/2</i> mutations	HNPCC (Lynch syndrome)	HNPCC (Lynch syndrome)	?	?
Precursors lesions	STIC	Atypical endometriosis	Atypical endometriosis	M-BTO	S-BTO
Chemosensitivity	High	High	Low	Low	Intermediate
Prognosis	Poor	Favorable	Intermediate	Favorable	Intermediate
Molecular abnormalities	<i>TP53</i> (96%), <i>BRCA1/2</i> (22%), chromosomal instability, <i>NF1</i> , <i>RB1</i> , <i>CDK12</i>	<i>CTNNB1</i> , <i>MSI</i> (12-20%), <i>PTEN</i> (20%), <i>ARID1A</i> , <i>KRAS</i> , <i>PIK3CA</i>	<i>ARID1A</i> (50%), <i>PIK3CA</i> , <i>PTEN</i> , <i>mTOR</i> , <i>KRAS</i>	<i>KRAS</i> , <i>HER2</i>	<i>BRAF</i> (38%), <i>KRAS</i> (19%), <i>NRAS</i> , <i>HER2</i> , <i>FGFR2</i>

HGSC, high-grade serous carcinoma; EC, endometrioid carcinoma; CCC, clear cell carcinoma; MC, mucinous carcinoma; LGSC, low-grade serous carcinoma; HNPCC, hereditary nonpolyposis colorectal cancer; STIC, serous tubal in situ carcinoma; M-BTO, mucinous borderline tumor of the ovary; S-BTO, serous borderline tumor of the ovary.

Fifteen years ago, a new classification was proposed dividing EOC into type I and type II tumors. Type I includes low-grade serous, low-grade endometrioid, mucinous, clear cell and malignant Brenner carcinomas. These tumors are usually confined to the ovary and are characterized by clearly defined precursors and slow progress from adenoma, often through the borderline tumor, to the corresponding carcinoma. They are relatively genetically stable with isolated mutations. The most common alterations in this type are *KRAS*, *BRAF* and *ERBB2* mutations; less often *PTEN*, *PIK3CA*, or *CTNNB1* are mutated. Type II ovarian carcinomas consist mostly of high-grade serous tumors, and relatively uncommon malignant mixed Müllerian tumors and undifferentiated carcinomas. They are highly aggressive tumors almost always diagnosed at advanced stage. These tumors are genetically unstable

and characterized by frequent *TP53* and *BRCAl/2* mutations, but rarely display mutations typical for type I tumors. (Shih et Kurman, 2004)

Originally, the ovary was thought to be the primary site of OC tumorigenesis with the ovarian surface epithelium (mesothelium) as the cell of origin. Despite the effort dedicated to finding precursor lesions within the ovary, none have been discovered and it was proposed that OC develop de novo. Recently, the evidence that ovarian tumors actually originate in non-ovarian tissue has accumulated. It has been proposed that serous tumors arise from the implantation of epithelium from the fimbriated end of fallopian tube (müllerian tissue), and endometrioid and clear cell carcinomas develop from endometriosis as a result of retrograde menstruation. The supposed origin of mucinous tumors is not well established, but it is assumed that these tumors could arise from transitional cell nests at the tubal-mesothelial junction near peritoneum. (Kurman et Shih, 2010)

The precise cause of OC is unknown, but several contributing factors have been identified. Like in any type of cancers the risk of developing OC increases with age. Family history of OC or breast cancer and inherited cancer syndromes, such as Lynch syndrome or mutations in *BRCAl* and *BRCAl2* genes, considerably increase the risk of OC. Nulliparity or late first pregnancy, early menarche and late menopause are also established risk factors. On the other hand, multiply pregnancy and breastfeeding, or use of contraceptive pills, seem to have protective effect. Other risk factors for OC include obesity, tall height, endometriosis, and the use of postmenopausal hormone therapy. (Jelovac et Armstrong, 2011)

1.1.3 Symptoms, diagnosis and treatment

OC, especially at early stages, is often asymptomatic or causes minimal vague symptoms. Nonspecific symptoms, easily dismissed or mistaken for more common conditions, may involve abdominal bloating or swelling, pelvic or abdominal pain, urinary symptoms (urgency or frequency), loss of appetite, digestive disturbances (indigestion, diarrhea, constipation), unexplained weight loss, extreme fatigue, or menstrual irregularities. At more advanced stages OC presents with ovarian, pelvic or abdominal mass and bowel obstruction, ascites and pleural effusion. (Berek et al., 2018)

If OC is suspected, a detailed medical history of patient and history of OC or any other cancer must be considered to assess possible risk factors. Then a complete physical examination including general, breast, pelvic, and rectal examination must be performed, followed by transvaginal ultrasonography and chest x-ray. MRI (Magnetic Resonance Imaging), CT (Computed Tomography) or PET (Positron Emission Tomography) can be used to complement ultrasonography and for detection of extraovarian spread (Fischerová et al., 2012). In addition to physical examination and imaging blood tests are done. They include blood typing test, common hematology tests, biochemical tests of hepatic and kidney profile and tumor marker detection (CA125, HE4, CEA, CA72-4, CA19-9, AFP, HCG).

A quantitative test ROMA (Risk of Ovarian Malignancy Algorithm) combines the test results of CA-125 and HE4 together with the menopausal status of the patient into a numerical score (Moore et al., 2009). It is used to determine the likelihood of malignancy and for differentiating between low- and high-risk patients with OC.

After the diagnosis of OC the stage needs to be determined. The main purpose of staging is to assign patients to the groups based on prognosis and most suitable treatment, and to provide standard terminology for statistical comparison. The currently used staging system is based on the FIGO (Fédération Internationale de Gynécologie et d'Obstétrique; International Federation of Obstetrics and Gynecology) classification of ovarian, fallopian tube, and peritoneum cancer (Berek et al., 2018), and the Union for International Cancer Control TNM pathological classification (Gospodarowicz et al., 2017). They both use 3 factors to stage cancer: the size of the tumor (T), the spread to nearby lymph nodes (N), and the spread (metastasis) to distant sites (M). FIGO staging system compared to TNM classification is presented in Appendices in Table A2.1.

Treatment options for patients with OC depend on several factors including the type and stage of OC, patient's age, overall health, and the personal preferences regarding future fertility. There are also different options whether it is primary, maintenance or recurrent OC therapy. The current standard treatment consists of primary cytoreductive surgery followed by an adjuvant platinum-based chemotherapy (carboplatin, cisplatin) combined with taxane (paclitaxel, docetaxel). In case of inoperability at the time of diagnosis patients undergo neoadjuvant chemotherapy followed by an interval debulking surgery.

Patient response to the initial platinum-based therapy is classified according to the platinum-free interval (the time period from end of treatment to relapse) into four categories: platinum-refractory (4 weeks), platinum-resistant (less than 6 months), partially platinum sensitive (6–12 months), and platinum sensitive (more than 12 months) (Stuart et al., 2011).

Targeted therapy is often used in addition to systemic chemotherapy or as an alternative therapy in recurrent or persistent OC. Currently available targeted therapies include angiogenesis inhibitors, such as monoclonal antibody bevacizumab, and poly (adenosine diphosphate-ribose) polymerase inhibitors (PARP inhibitors), such as olaparib or niraparib (PDQ Adult Treatment Editorial Board, 2019). Other treatments may include radiation therapy and immunotherapy.

1.1.4 Epithelial-mesenchymal transition in ovarian cancer

OC is a highly invasive and metastatic disease. Metastatic spread of tumor cells is enabled by epithelial-mesenchymal transition (EMT). During EMT, epithelial cells lose their polarity and cell-cell adhesion and acquire migratory characteristics of mesenchymal cells. This transition occurs physiologically during the developmental processes, such as embryo formation or tissue development (type I EMT), or repair processes, such as wound healing, tissue regeneration and organ fibrosis (type II EMT). Type III EMT is associated with cancer progression and metastasis. (Thiery et al., 2009)

In OC, the ability to induce EMT is attributed to transforming growth factor β (TGF- β), epidermal growth factor (EGF), hepatocyte growth factor (HGF) and endothelin-1 (ET-1) (Vergara et al., 2010). Several transcription factors are then activated, including SNAIL and SLUG family, and zinc finger E-box binding homeobox proteins (ZEB), as transcriptional repressors of E-cadherin. A key feature of EMT is thus the switch from E-cadherin to N-cadherin. Cells undergoing EMT display decreased expression of E-cadherin and zona occludens 1 protein (epithelial markers) accompanied by an increased expression of N-cadherin and vimentin (mesenchymal markers). (Lamouille et al, 2014)

1.1.5 High-grade serous ovarian carcinoma

The most common histological type accounting for up to ~ 80% of advanced EOC is an invasive serous carcinoma, recently subdivided into two distinct disease entities, high-grade and low-grade serous carcinomas (Vang et al., 2009). Originally, the ovary was thought to be the primary site of high-grade serous ovarian carcinoma (HGSOC) tumorigenesis with the ovarian surface epithelium as the cell of origin. In recent years, however, there has been emerging evidence that the majority of HGSOC (~ 60 %) originates in the fimbria of the fallopian tube and arises from STIC (serous tubal intraepithelial carcinomas) (Lee et al., 2007; Vang et al., 2013). Implantation of fallopian tube-like epithelium to the ovary (endosalpingiosis) and possibly inclusions of the ovarian surface epithelium are considered the site of origin for the rest of HGSOC (Zeppernick et al., 2015).

HGSOC is characterized by an advanced stage at onset, nearly universal occurrence of mutation in the *TP53* gene, mutations in the homologous recombination DNA repair pathway (*BRCA1* and *BRCA2* genes) and widespread copy number alterations (Cancer Genome Atlas Research Network, 2011). While mutations of *BRCA1* and *BRCA2* are typical for familial HGSOC, inactivation of these genes in sporadic HGSOC is frequently caused by other mechanisms, such as hypermethylation of gene promoters. DNA copy number alternations associated with HGSOC often include cyclin E1 (*CCNE1*), *NOTCH3*, *AKT2*, *RSF1*, and *PIK3CA* loci (Kurman et Shih, 2011). Based on differences in mRNA and miRNA expression and DNA methylation profiles the Integrated genomic analysis of OC further divided HGSOC into four subtypes: (1) immunoreactive (characterized by T-cell chemokine ligands *CXCL10/11*, and the receptor *CXCR3*), (2) differentiated (associated with high expression of *MUC1/16*, and with expression of secretory fallopian tube marker *SLPI*), (3) proliferative (defined by high expression of transcription factors *HMGA2* and *SOX11*, and proliferation markers *MCM2* and *PCNA*, and by low expression of *MUC1/16*), and (4) mesenchymal (characterized by high expression of *HOX* genes and markers *FAP* and *ANGPTL1/2*). Pathways deregulated in HGSOC include known cancer-associated pathways, such as RB, RAS/PI3K, FOXM1, and NOTCH. (Cancer Genome Atlas Research Network, 2011)

In most cases, HGSOC is treated with a combination of carboplatin and paclitaxel with initial response rates of 60–80% (Selvakumaran et al., 2003).

However, despite the relatively high initial response, majority of patients become platinum resistant with subsequent relapses. Ultimately, almost all HGSOC patients develop platinum resistance and succumb to the disease (Davis et al., 2014). To date, the complete set of mechanisms underlying HGSOC platinum chemotherapy resistance and how they interact is not fully understood. The most studied mechanisms include genome-wide mutations, epigenetic changes and dysfunctional DNA repair. Probably working together, they lead to genomic instability that allows cancer cells either to adapt and survive DNA damage caused by platinum chemotherapy or prevent entry into the cell, eventually expel the drug. The presence of cancer stem cells, EMT and tumor microenvironment (immune cell infiltration, angiogenesis and hypoxia) have also been implicated in platinum resistance (Van Zyl et al., 2018).

1.2 Epigenetics in ovarian cancer

Similar to other malignancies, OC is considered to be driven by progressive genetic alterations, such as mutations in oncogenes or tumor suppressor genes, as well as chromosomal abnormalities. It has been confirmed that also epigenetic alterations significantly contribute to the OC initiation and progression (Barton et al., 2008). These alternations refer to the heritable modification of DNA without any change in its nucleotide sequence. They affect gene activity and expression and are associated with a phenotype.

1.2.1 DNA methylation

One of the most common epigenetic events taking place in a mammalian genome is DNA methylation. It refers to the covalent addition of a methyl group to the 5-carbon of cytosine ring in CpG sequences resulting in 5-methylcytosine (Figure 3). The methyl group is transferred from S-adenosylmethionine in the reaction catalyzed by DNA methyltransferases (DNMTs). DNMT3A and DNMT3B are responsible for de novo DNA methylation, and DNMT1 functions as the maintenance methyltransferase that copy DNA methylation patterns during DNA replication (Jones et Baylin, 2002).

In tumor cells, DNA methylation is usually redistributed between global genomic hypomethylation and localized CpG island hypermethylation.

Hypermethylation that occurs in the promoter regions of tumor suppressor genes or genes involved in the cell cycle control, apoptosis and drug sensitivity, results in transcriptional silencing (Barton et al., 2008). Aberrant methylation of CpG islands in the promoter region of various genes associated with OC has been observed in numerous studies (Koukura et al., 2014; Zhang et al., 2014; Huang et al., 2013).

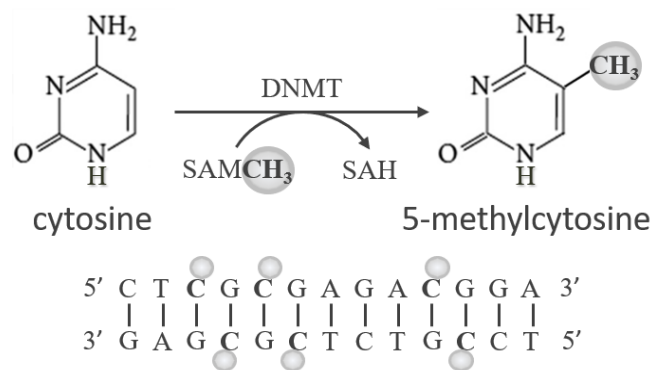


Figure 3 Schematic representation of DNA methylation. DNMT, DNA methyl transferase; SAM, S-adenosylmethionine, SAH, S-adenosylhomocysteine.

Methods for detecting DNA methylation

Numerous techniques are currently used to detect and quantify DNA methylation. When selecting the most suitable method for particular study, several factors should be considered. The decision is based mainly on the project's purpose and the aims that have been set (e.g. whether quantitative or qualitative analysis is required, whether it is genome-wide profiling study or study focused on locus-specific methylation). The amount and quality of analyzed samples, as well as sensitivity and specificity requirements of the project must be taken into consideration. Extremely important is to consider the required bioinformatic capability for data analysis and interpretation. Other factors that affect the selection include labor intensity and difficulty of the method, the availability of specialized equipment and reagents, and last but not least, the cost-effectivity of the selected method. (Kurdyukov et Bullock, 2016)

According to the methylation-dependent treatment prior to analysis itself, a wide spectrum of the DNA methylation analysis methods can be classified into three main groups: (1) bisulfite conversion-based, (2) restriction enzyme-based and (3) affinity

enrichment-based strategies. The overview of available methods in each group, as reviewed by Olkhov-Mitsel and Bapat (2012), is provided below.

1. Methods based on bisulfite conversion

Methods relying on bisulfite treatment are most widely accepted and used approaches for methylation analysis. Bisulfite conversion involves chemical modification of unmethylated cytosines to uracils, while methylated cytosines remain unchanged. In subsequent analysis, methylated cytosines are thus detected as cytosines, whereas unmethylated cytosines converted to uracils are detected as thymines.

The most comprehensive genome-wide approach for DNA methylation profiling is WGBS (Whole genome bisulfite sequencing). It provides single base-pair resolution, but requires high DNA input and is quite expensive (Lister et al., 2009). The alternative can be RRBS (Reduced representation bisulfite sequencing), where DNA is at first cleaved by restriction enzymes, and only fragments containing CpG-rich regions then undergo bisulfite conversion and sequencing (Meissner et al., 2005). Other alternative methods are DHPLC (Denaturing high-performance liquid chromatography) or BiMP (Bisulfite methylation profiling) microarrays (Baumer et al., 2001; Reinders et al., 2008).

Where targeted locus-specific analysis is required, one of the following strategies is usually employed:

- ~ BSP, Bisulfite sequencing PCR (bisulfite converted DNA, BC DNA, is PCR amplified and sequenced) (Frommer et al., 1992),
- ~ MSP, Methylation-specific PCR (BC DNA is amplified with primers specific either for methylated or unmethylated sequence, then analyzed by gel electrophoresis) (Herman et al., 1996),
- ~ MethylLight (BC DNA is amplified with methylation specific primers and a fluorescent probe) (Eads et al., 2000),
- ~ HeavyMethyl (oligonucleotide blockers prevent amplification of unmethylated DNA, methylated DNA is amplified with methylation independent primers and a fluorescent probe) (Cottrell et al., 2004),
- ~ MS-MCA, Methylation-sensitive melting curve analysis and MS-HRM, Methylation-sensitive high-resolution melting (employ a fluorescent dye

to monitor the melting properties of PCR products following MSP) (Worm et al., 2001; Wojdacz et Dobrovic, 2007),

- ~ SMART-MSP, Sensitive melting analysis after real-time methylation-specific PCR (amplification of BC DNA with methylation specific primers and a fluorescent dye is followed by HRM) (Kristensen et al., 2008).

Less common bisulfite-based methods for targeted locus-specific analysis of methylation may include:

- ~ MS-SnuPE, Methylation sensitive single nucleotide primer extension (BC DNA is amplified with primers that terminate after the cytosine of interrogated CpG, and then the ratio C to T is determined) (Gonzalvo et Jones, 1997),
- ~ MS-FLAG, Methylation-specific fluorescent amplicon generation (employs methylation specific primers labeled with fluorophore, that release a fluorescence signal upon digestion with *PspGI*) (Bonanno et al., 2007),
- ~ GoldenGate (BC DNA is subjected to whole genome amplification and microarray hybridization) (Bibikova et al., 2006),
- ~ MassARRAY EpiTYPER (BC DNA with a T7-promoter tag is transcribed and digested with *RNaseA*, then analyzed by MALDI-TOF-MS) (Ehrich et al, 2005),
- ~ BSPP, Bisulfite padlock probes (employs set of padlock probes to capture BC DNA) (Deng et al., 2009).

2. Methods based on restriction enzyme digestion

Restriction enzyme-based methods take advantage of restriction enzymes ability to digest only unmethylated DNA (in case of methylation-sensitive restriction enzymes, such as *HpaII* or *HhaI*) or methylated DNA (in case of methylation-dependent restriction enzymes, such as *MspI*).

Most common sequencings strategies for genome-wide DNA methylation profiling using restriction enzymes are:

- ~ RLGS, Restriction landmark genome scanning (Hatada, 1991),
- ~ HELP-Seq, *HpaII* tiny fragment enrichment by ligation-mediated PCR (Oda et al., 2009),
- ~ LUMA, Luminometric methylation (Karimi et al. 2006),
- ~ MSCC, Methylation-sensitive cut counting (Ball et al., 2009),

- ~ MCA, Methylated CpG island amplification (Toyota et al., 1999),
- ~ and Methyl-Seq (Brunner et al., 2009).

Genome-wide restriction enzyme-based strategies that utilize microarrays hybridization include:

- ~ HELP, *Hpa*II tiny fragment enrichment by ligation-mediated PCR (Khulan et al., 2006),
- ~ MCAM, Methylated CpG island amplification microarray (Estecio et al., 2007),
- ~ MAD, Methylation amplification DNA chip, and PMAD, Promoter-associated methylated DNA amplification DNA chip (Hatada et al., 2002; Fukasawa et al., 2006),
- ~ CHARM, Comprehensive high-throughput arrays for relative methylation (Irizarry et al., 2008),
- ~ Mmass, Microarray-based methylation assessment of single samples (Ibrahim et al., 2006),
- ~ DMH, Differential methylation hybridization (Huang et al., 1999),
- ~ MSNP, Methylation single-nucleotide polymorphism (Kerkel et al., 2008),
- ~ and MethylScope (Ordway et al., 2006).

For locus-specific analysis are suitable Methylation-sensitive arbitrarily primed PCR (MS-AP-PCR) and Amplification of intermethylated sites (AIMS). In these methods, digested DNA is radioactively labeled and analyzed by gel electrophoresis and autoradiography (Gonzalzo et al., 1997; Frigola et al., 2002). Another widely used restriction enzyme-based method is Methylation-specific multiplex ligation-dependent probe amplification (MS-MLPA). This technique is based on digestion of unmethylated CpG after probe hybridization and ligation, followed by PCR amplification and capillary electrophoresis (Nygren et al., 2005).

3. Methods based on affinity enrichment

Affinity enrichment of methylated DNA is the main principle of Methylated DNA immunoprecipitation (MeDIP) and Methylated CpG island recovery assay (MIRA) (Weber et al., 2005; Rauch et Pfeifer, 2005). In MeDIP, single-stranded DNA is immunoprecipitated with anti-5-methylcytosine antibodies; MIRA utilize MBD2b/MBD3L1 protein complex to bind methylated DNA. Sequencing or microarray platforms can be employed in both of these methods.

Combination of bisulfite conversion-based and enzyme restriction-based approach is utilized in COBRA (Combined bisulfite restriction analysis), where BC DNA is amplified using methylation independent primers and then digested with *Bst*UI (Xiong et Laird, 1997). Another method that employs two of three main techniques is COMPARE-MS (Combination of methylated DNA precipitation and methylation-sensitive restriction enzymes) (Yegnasubramanian et al., 2006). This approach can increase specificity and sensitivity in targeted locus specific analysis of methylation.

1.2.2 Posttranscriptional regulation by microRNA

Next widely studied area of epigenetics are microRNAs (miRNAs). According to the miRNA database (miRBase), over 2 600 mature miRNAs have been identified in humans so far (Kozomara et al., 2019). They represent a class of small, endogenous, ~22 nucleotides long non-coding RNA molecules that are involved in gene expression regulation of important cellular processes, such as cell proliferation, differentiation, angiogenesis, migration and apoptosis. Primary function of miRNAs at the post-transcriptional level is repression of translation via RNA interference as part of the RNA-induced silencing complex (RISC) (Bartel, 2004). Number of studies have associated dysregulation of various miRNAs to OC development and progression and indicated that miRNA expression profiles can be potentially used as diagnostic and prognostic biomarkers, or in prediction of patients' response to treatment (Di Leva et al., 2013; Ferracin et Negrini, 2015; Sorrentino et al., 2008).

Deregulated miRNAs associated with diagnosis of various type of OC, as reviewed by Katz et al. (2015) and updated with current data, are summarized in the following tables. Table 2 shows alterations of miRNA expression levels in ovarian tissue compared to normal ovarian surface epithelium. Deregulated miRNAs detected in blood (plasma/serum) of OC patient compared to healthy controls are presented in Table 3. Zavesky et al. (2015) investigated cell-free miRNA expression in urine as well and found miR-92a to be significantly up-regulated, and miR-106b significantly down-regulated in comparison to control samples.

Table 2 Deregulated miRNAs detected in ovarian tissue associated with diagnosis of various types of ovarian cancer (adapted from Katz et al., 2015)

Histology	Deregulated miRNAs	Reference
Various types	↑ miR-200a, miR-141 ↓ miR-199a, miR-140, miR-145, miR-125b	Iorio et al., 2007
SC, EC, CCC	↑ miR-126*, miR-195, miR-200b, miR-338-3p, miR-142-3p, miR-200a, miR-200c, miR-378* ↓ miR-100, miR-210, miR-222, miR-409-5p, miR-493, miR-127-3p, miR-22, miR-382, miR-485-5p	Wyman et al., 2009
SC	↑ miR-205, miR-429, miR-141 ↓ miR-320a, miR-383	Shahab et al., 2012
SC	↑ miR-200c, miR-141, miR-93 ↓ let-7b, miR-99a, miR-125b	Nam et al., 2012
CCC	↑ miR-30a/30a*	Calura et al., 2013
MC	↑ miR-192/194	
HGSC	↑ miR-141-3p, miR-182-5p, miR-200a-3p, miR-200a-5p, miR-200b-3p, miR-200c-3p, miR-205-5p ↓ miR-134, miR-202-3p, miR-383, miR-424-5p, miR-509-5p, miR-509-3-5p	Vilming Elgaaen et al., 2014
CCC	↑ miR-141-3p, miR-182-5p, miR-200a-3p, miR-200a-5p, miR-200b-3p, miR-200c-3p, miR-508-5p, miR-509-5p, miR-510, miR-513a-5p, miR514b-5p ↓ miR-383, miR-424-5p	
EC	↑ miR-93-5p, miR-141-3p, miR-429, miR-200c-3p, miR-492	Braicu et al., 2017
SC	↓ miR-4443, miR-5195-3p	Ebrahimi et Reisi, 2019

SC, serous carcinoma; EC, endometrioid carcinoma; CCC, clear cell carcinoma; MC, mucinous carcinoma; HGSC, high-grade serous carcinoma.

Table 3 Deregulated miRNAs detected in blood associated with diagnosis of various types of ovarian cancer (adapted from Katz et al., 2015)

Histology	Deregulated miRNAs	Reference
SC, EC, CCC, MC	↑ miR-21, miR-29a, miR-92, miR-93, miR-126 ↓ miR-127, miR-155, miR-99b	Resnick et al., 2009
SC, EC	↑ miR-30c1* ↓ miR-342-3p, miR-181a*, miR-450b-5p	Hausler et al., 2010
Various types	↑ miR-205 ↓ let-7f	Zheng et al., 2013
SC	↓ miR-132, miR-26a, let-7b, miR-145	Chung et al., 2013
SC	↑ miR-1274a, miR-625-3p, miR-720 ↓ miR-106a, miR-126, miR-146a, miR-150, miR-16, miR-17, miR-19b, miR-20a, miR-223, miR-24, miR-92a, miR-106b, miR-191, miR-193a-5p, miR-30b, miR-30a-5p, miR-30c, miR-320, miR-328	Shapira et al., 2014
SC	↓ let-7i-5p, miR-152, miR-122-5p, miR25-3p	Langhe et al., 2015
HGSC	↑ miR-200a, miR-200b, miR-200c	Kan et al., 2015
HGSC	↑ miR-1246, miR-595, miR-2278	Todeschini et al., 2017

SC, serous carcinoma; EC, endometrioid carcinoma; CCC, clear cell carcinoma; MC, mucinous carcinoma; HGSC, high-grade serous carcinoma.

1.2.3 Histone modifications

Other epigenetic alterations that play a key role in the gene transcription regulation of cancer cells are histone modifications, covalent post-translational modifications of histone proteins, which include acetylation, phosphorylation, methylation, ubiquitylation, and sumoylation. These modifications can influence gene expression by direct remodeling of chromatin structure or by recruiting histone modifiers (Bannister et Kouzarides, 2011). The most widely studied histone modification is acetylation, enzymatic addition of acetyl group from acetyl coenzyme A. It is regulated by two classes of enzymes, histone acetyltransferases (HATs) and histone deacetylases (HDACs). HDACs are often overexpressed in cancer cells, resulting in altered expression and activity of proteins involved in carcinogenesis. High levels of HDAC1, 2 and 3 have been identified also in OC tissues (Jin et al., 2008). Overexpression of class I HDACs in OC has been associated with poor prognosis (Weichert, et al. 2008) and implicated in metastatic process (Hayashi et al.,

2010). Their role in development of platinum resistance in OC cell lines has been also confirmed (Kim, MG et al., 2012).

1.2.4 Epigenetic therapy of ovarian cancer

The reversibility of epigenetic changes brings new possibilities into the search for improved cancer therapy. Number of epigenetic drugs is currently being investigated for their potential to reverse unfavorable epigenetic alterations associated with OC. The most successful epigenetic therapies to date are DNMT inhibitors 5-azacitidine and decitabine (5-aza-2'-deoxycytidine), initially developed as cytotoxic drugs for treatment of hematologic malignancies (Moufarrij et al., 2019). Less toxic drugs, such as zebularine or the small-molecule inhibitor RG108 are being tested as replacement. Other intensively investigated epigenetic agents are HDAC inhibitors. Their development was initiated by the discovery that sodium butyrate can act as an inhibitor of HDAC activity. For use in OC, HDAC inhibitors belinostat, vorinostat or romidepsin have been tested (Smith et al., 2017).

Both HDAC inhibitors and DNMT inhibitors have been investigated as single agents or combined with other therapies. While response to single-agent epigenetic therapy has been low so far, combination with other drugs may be promising (Ahuja et al., 2016). Epigenetic agents in combination with drugs commonly used in OC therapy have been able to improve response to immunotherapy or sensitize patients to platinum-based therapy. Pretreatment with azacytidine or decitabine produced higher response rates to re-treatment with platinum in patients with platinum-resistant OC. It led to demethylation of tumor suppressor genes *MLH1*, *RASSF1A*, *HOXA10*, and *HOXA11*, hypermethylation of which has been associated with the development of platinum resistance. (Matei et al., 2012)

Two clinical trials are currently enrolling patients for testing new combinations of epigenetic drugs for treatment of recurrent or non-responsive epithelial ovarian, fallopian tube, or primary peritoneal carcinoma. The one is in phase I and studies the side effects of genetically modified T cells and decitabine; the second one (phase I/IIb) studies side effects and best dose of atezolizumab when given together with DNMT inhibitor guadecitabine and CDX-1401 vaccine. (PDQ Adult Treatment Editorial Board, 2019)

1.3 Adhesion molecules

Cell adhesion molecules (CAMs) are integral membrane proteins that take part in intercellular and cell-to-extracellular matrix interactions. They regulate or significantly contribute to a variety of functions including signal transduction, cell growth and differentiation, morphogenesis, site specific gene expression, immunologic function, cell motility, wound healing, or inflammation (Okegawa et al., 2004). Alterations in cell adhesion can disrupt important cellular processes and lead to various diseases, including cancer, where CAMs participate in tumor invasiveness and metastasis.

All of CAMs comprise of extracellular, transmembrane and cytoplasmic domains. The cytoplasmic domain anchors CAMs to the cytoskeletal proteins, while extracellular domain interacts with matrix or ligands on adjacent cells. Based on their protein structure, CAMs can be divided into four main groups: the integrin family, the immunoglobulin superfamily, selectins, and cadherins (Figure 4).

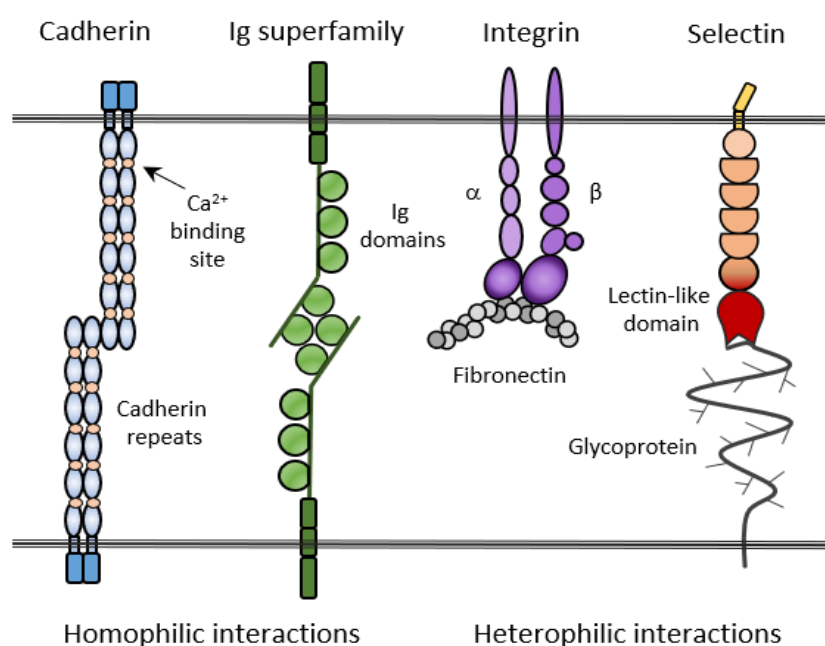


Figure 4 Major families of cell adhesion molecules.

Integrins are heterodimeric transmembrane receptors, formed by α and β subunits, that can mediate both cell-to-cell and cell-to-matrix interaction with extracellular proteins collagen, fibrinogen, fibronectin, and vitronectin (Humphries

et al., 2006). By modifying their intracellular domains, integrins can regulate affinity of their ligands. On the other hand, the ligands binding to integrin extracellular domains can induce conformational changes and initiate thus signaling cascades (Takada et al., 2007).

The immunoglobulin CAMs contain transmembrane proteins with one or more immunoglobulin-like domains in their extracellular domains that can bind to either other members of immunoglobulin superfamily (homophilic, such as neural CAMs) or integrins (heterophilic, such as intercellular CAMs or vascular CAMs) (Wai Wong et al., 2012).

Selectins are single-chain transmembrane glycoproteins containing calcium-dependent lectin domain. They are expressed on the surface of leukocytes (L-selectin), platelets (P-selectin) and activated endothelial cells (E-selectin and P-selectin). They play important role in lymphocyte homing, and in chronic and acute inflammation processes (Ley, 2003).

Cadherins are calcium-dependent transmembrane glycoproteins that mediate cell-to-cell adhesion in almost all type of tissue. The extracellular domain, consisting of several cadherin repeats, binds in homophylic interaction to another cadherin. The intracellular domain is anchored via cytoplasmatic proteins (catenins) to the actin cytoskeleton, allowing thus stabilization and dynamic regulation of the junction (Dejana, 2004). The cadherin superfamily includes classical cadherins, protocadherins, desmosomal and unconventional cadherins. Classical cadherins have five cadherin repeats and are involved in significant signaling pathways, such as Wnt or hedgehog. The most widely studied are epithelial (E)-cadherin, neural (N)-cadherin, and placental (P)-cadherin. Protocadherins have more than five cadherin repeats and are thought to be related to ancestral cadherin, though they do not attach to the cytoskeleton trough catenins. They are highly variable, with a variety of function, mostly in the nervous system. Based on their genomic structure protocadherins are subdivided into clustered and non-clustered groups. The clustered protocadherins, comprising the α , β , and γ groups, are arranged in tandem on a single chromosome. The non-clustered protocadherins are located on multiple chromosomes at three different chromosomal loci and divided into $\delta 1$, $\delta 2$, and ϵ groups. Desmosomal cadherins are involved in forming cellular junctions, desmosomes. They include desmogleins and desmocollins. Unconventional cadherins are otherwise uncaterogized cadherins,

such as vascular endothelial (VE)-cadherin or retinal (R)-cadherin. (Angst et al., 2001; Morishita and Yagi, 2007)

Cadherins downregulation or absence in malignant cells has been associated with carcinogenesis and cancer progression. Current studies showed aberrant DNA methylation of various classical cadherin genes in human malignant tumors (Asiaf et al., 2014; Wu et al., 2014; Lin et al., 2015). The tumor suppressor role of protocadherins has been recently affirmed as well (Shan et al., 2016). Moreover, different studies have confirmed the significance of altered methylation of protocadherins in various types of cancers (Tang et al., 2012; Luo et al., 2014; Niu et al., 2014; Yin et al., 2016).

2 Objectives

The following objectives were specified for this study:

1. Optimization of methods for monitoring DNA methylation changes in genes encoding adhesion molecules using next-generation sequencing.
2. Optimization of real-time PCR-based methods for confirmation of the previously detected most significant alterations in the methylation status.
3. Methylation analysis of selected adhesion molecule genes in high-grade serous ovarian carcinoma tissue in comparison with control tissue.
4. Correlation of detected methylation changes to clinicopathological characteristics and follow-up data of the patients.
5. Design of potential biomarker panel based on DNA methylation for future use in ovarian cancer screening.

3 Materials and Methods

3.1 Study group

Study group was selected from patients treated at the Department of Obstetrics and Gynecology, University Hospital Hradec Králové, between years 2001-2018. It consisted of 68 patients with HGSOE and 46 patients who had undergone surgery for non-malignant diagnosis, such as uterine fibroids or descent of uterus with adnexectomy. The study was approved by the Ethics Committee of University Hospital Hradec Králové and conducted in accordance with the Declaration of Helsinki. Informed consent was obtained from each concerned patient. Of the 114 initially enrolled patients, 10 patients were excluded from analyses due to the insufficient amount of obtained tissue or poor-quality tissue.

The set of analyzed samples contained 103 samples of formalin-fixed, paraffin-embedded (FFPE) tissue from ovary or the fallopian tube fimbria epithelium (in case of control samples) and 32 fresh frozen samples of ovary. All samples were reviewed and classified according to the current WHO classification of tumors of female reproductive organs by an experienced gynecopathologist.

Stage I or II was classified in 23.0 % (14/61) of tumors, 77.0 % (47/61) of tumors were stage III or IV, with stage III.C as the most prevalent (61 %). Detailed distribution of tumors stages is presented in Figure 5.

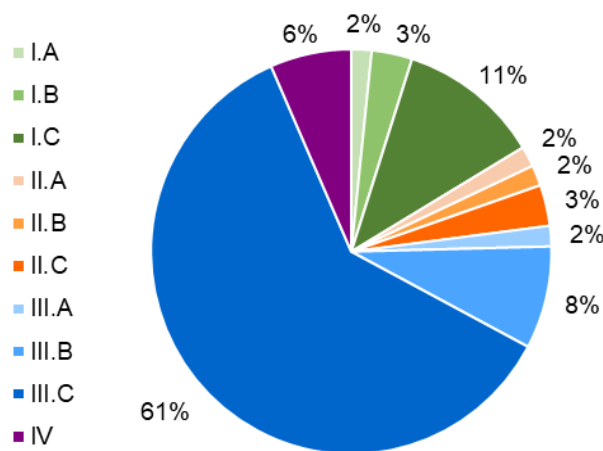


Figure 5 Distribution of tumor stages in study group.

The median age at the time of HGSOC diagnosis was 58 years (40–79 years); median age at the time of surgery in control group was 57 years (42–84 years). Age distribution of study group is shown in Figure 6.

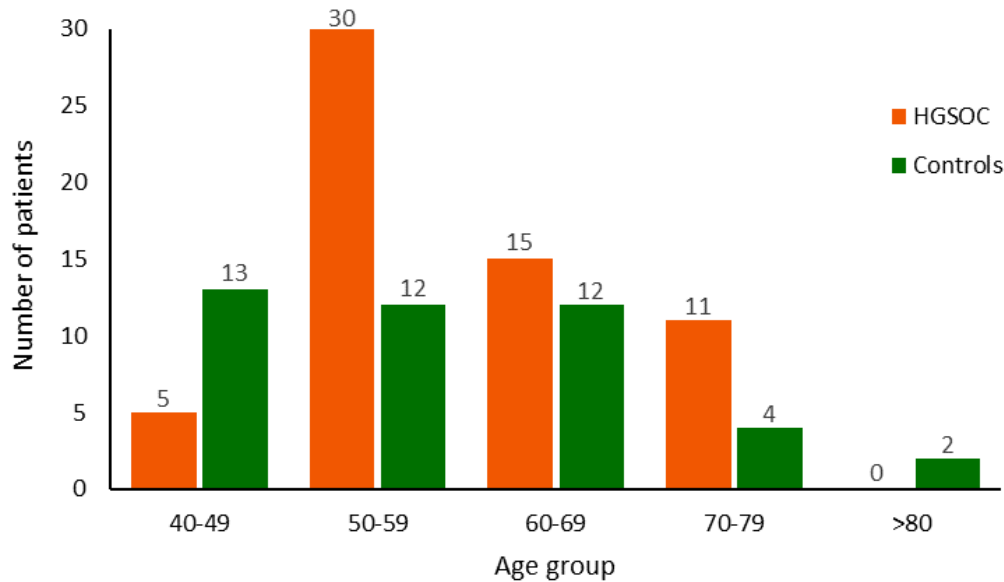


Figure 6 Age distribution of study group.

3.2 DNA extraction

Genomic DNA was extracted using silica-membrane-based QIAmp DNA Mini Kit (Qiagen, Hilden, Germany) according to the manufacturer's instruction. Initial processing of different tissue samples preceded the extraction procedure. In case of FFPE tissue, the samples were first deparaffinized with xylene and washed with 96% ethanol. Fresh frozen samples underwent mechanical tissue homogenization using lysis buffer and glass beads in the MagNA Lyser Instrument (Roche, Basel, Switzerland) for 60 second at 6,000 rpm. The DNA extraction then followed the same procedure in both types of samples. Overnight lysis under denaturing conditions with proteinase K was followed by binding of DNA to the column membrane. Subsequent membrane washing removed all residual contaminants and pure DNA was eluted from the membrane. The purity of extracted DNA was examined spectrophotometrically on the NanoDrop 1000 Spectrophotometer (Thermo Fisher Scientific, Waltham, MA, USA). To assess DNA purity absorbance was measured at 260 nm, 280 nm and 230 nm. DNA was considered pure if 260/280 ratio was ~1.8

and the 260/230 value was at least 1.5. DNA was then quantified on the Qubit® Fluorometer (Thermo Fisher Scientific).

3.3 Bisulfite conversion of DNA

All of the methods used for detecting methylation in this study required bisulfite conversion of extracted DNA. Bisulfite treatment is one of the oldest techniques for analyzing DNA methylation and is still considered to be the gold standard. It involves chemical deamination of all unmethylated cytosines to uracils while leaving methylated cytosines unaffected. In subsequent polymerase chain reaction (PCR) uracils are amplified as thymines and originally methylated cytosines are recognized without change (Figure 7).

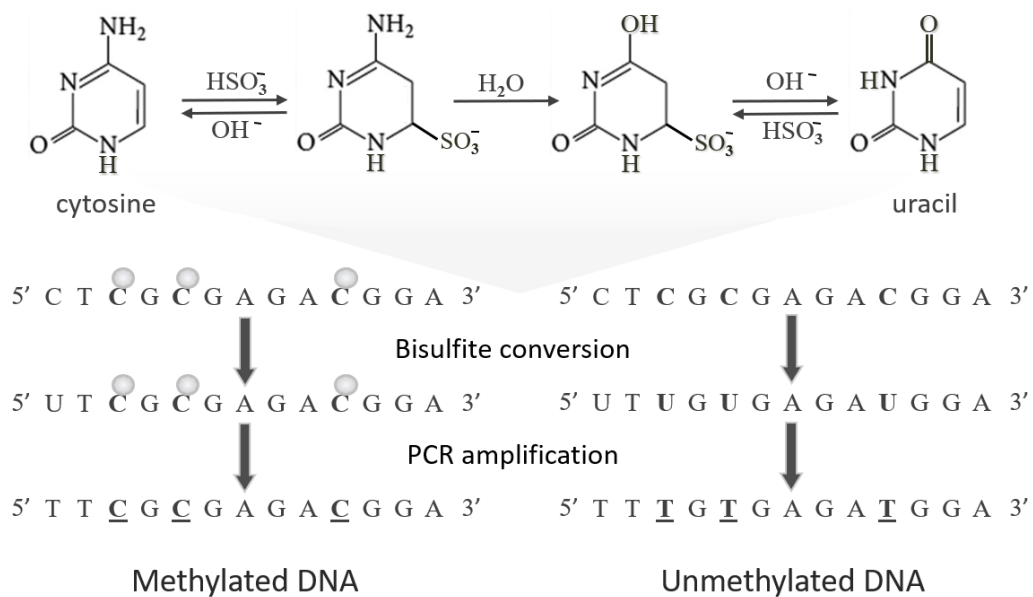


Figure 7 Schematic illustration of bisulfite conversion.

DNA was bisulfite-converted with EZ DNA Methylation-Gold™ Kit according to the manufacturer's protocol (Zymo Research Corporation, Irvine, CA, USA). Briefly, CT Conversion Reagent was added to 500 ng of genomic DNA; the mix was denatured for 10 minutes at 98 °C and incubated for 2.5 h at 64 °C. Samples were then transferred to columns with binding buffer and subsequently desulfonated, washed and eluted from the membrane.

3.4 Next-generation sequencing

The term next-generation sequencing (NGS) covers number of different modern high-throughput sequencing technologies. In this study Illumina platform with targeted amplicon sequencing approach was employed. Illumina NGS uses clonal amplification and reversible-terminator sequencing by synthesis technology and enables thus base-by-base sequencing with highly accurate data. In the process of incorporating DNA bases to the growing strand each base emits unique fluorescent signal which is used to determine the order of the DNA sequence. Targeted amplicon sequencing is cost-effective technique that allows focusing on selected regions of interest. This approach involves initial amplification of regions of interest in PCR followed by sequencing of the amplicons. In this study, altogether 16 amplicons in the following genes were analyzed: *CDH10* (amplicons *CDH10_1* and *CDH10_2*), *CDH13* (*CDH13*), *CDH18* (*CDH18_1* and *CDH18_2*), *PCDH8* (*PCDH8_1* and *PCDH8_2*), *PCDH10* (*PCDH10_1* and *PCDH10_2*), *PCDH17* (*PCDH17_1*, *PCDH17_2* and *PCDH17_3*), *CTNNA2* (*CTNNA2_1* and *CTNNA2_2*) and *CTNND2* (*CTNND2_S* and *CTNND2_L*). The gene regions were selected to cover gene promoter and first exon in the view of the CpG island predicted position. The amplicon length limitations of MiSeq sequencing chemistry was taken into account as well.

Specific primers for amplification were designed in the on-line methylation primer designing software MethPrimer (Li et Dahiya, 2002). The software is intended for designing primers that anneal to bisulfite modified DNA. It can also predict the position of CpG islands. To ensure unbiased amplification of both methylated and unmethylated DNA, primers for bisulfite sequencing should not contain any CpG sites. However, the density of CpG sites in selected regions in *CTNNA2* and *CTNND2* did not allow to design primers without any CpG. Therefore, degenerate bases Y (C or T) and R (A or G) were included in the primer sequences to enable primers anneal to DNA regardless of methylation status. Schematic location of primers relative to the investigated CpG sites is depicted in Figure 8A. For subsequent sequencing of amplicons, specific adaptor sequence was added to the designed primers. Amplicons information and primer sequences of each amplicon are listed in Table 4.

Table 4 Amplicon characteristics and primer sequences in next-generation sequencing

Amplicon name	Coordinates (strand)	Amplicon size ^s (bp)	CpGs/ Amplicon	Primer sequence 5´-3´ (with adapters*)
CDH10_1	hg19_chr5:24,645,171-24,645,476 (-)	306	7*	Fw: *TTTTGTGATAATAAGTAATAAGAGAAGGGA Rv: *TCAAACACTAAAATAATCAACCCAATCTA
CDH10_2	hg19_chr5:24,644,904-24,645,238 (-)	335	11*	Fw: *TAGTTTTGTTTTGAGATTGTATTA Rv: *TAATTAACCTTCATTCAACTTCTAATTA
CDH13	hg19_chr16:82,660,398-82,660,750 (+)	353	23	Fw: *TAATAGTTTAAAGAAGTAAATGGGATGTTA Rv: *TTCCTACCTAAAACAAAAAAC
CDH18_1	hg19_chr5:19,988,559-19,988,877 (-)	319	10	Fw: *TAGTAGTTGAATGTTTAGTAGGTTGTGA Rv: *CCCCTCAACAAAATCATATAAAAAA
CDH18_2	hg19_chr5:19,988,261-19,988,578 (-)	318	18	Fw: *TATATGATTTTTGTTGAGGGGGTTAA Rv: *CCCAAACTCTAAACACAACACTACTC
PCDH8_1	hg38_chr13:52,848,879-52,849,262 (-)	384	12	Fw: *TTTTTTTGAAGGGGAAGTGGTAGT Rv: *CAAACTCCA AAAAATAAAAAAAC
PCDH8_2	hg38_chr13:52,848,432-52,848,812 (-)	381	31	Fw: *AGAAAGATTTTTTAATTTTTTTT Rv: *CTCATACCTCCAACCTCAAATAC
PCDH10_1	hg38_chr4:133,149,215-133,149,575 (+)	361	10	Fw: *GGTGGGTGGTGTTTTTGG Rv: *ACTCTACAACCTAAAACCTTCATTCT
PCDH10_2	hg38_chr4:133,149,551-133,149,936 (+)	385	12	Fw: *AATGAAAGTTTTAAGTTGTAGAGT Rv: *TTAACACAAAAAAAATAACAAAC
PCDH17_1	hg38_chr13:57,631,479-57,631,871 (+)	393	16	Fw: *TTGTTTGGAGAGAAGTTTTTGT Rv: *ACATTTAAAAATCTAATCTTACATTA
PCDH17_2	hg38_chr13:57,631,872-57,632,271 (+)	400	22	Fw: *AGTAAATATTGTTTAAAAATAGAT Rv: *ACTAAAAATAAACCAAAAATTC
PCDH17_3	hg38_chr13:57,632,344-57,632,603 (+)	260	14	Fw: *TTGTAGATTAATAGGTTTAGGGAATT Rv: *CTTAAAAATAAAAACAAAAACCCATA
CTNNA2_1	hg38_chr2:79,512,646-79,512,803 (+)	158	15	Fw: *TTYGTTYGTAGGGTAAYGYG Rv: *ACCTAAAAACRCCCAA
CTNNA2_2	hg38_chr2:79,512,828-79,513,020 (+)	193	25	Fw: *TAGTTATTTTTYGATGTTYGGTG Rv: *AAACTAAAAACRAAACCRCTCC
CTNND2_S	hg38_chr5:11,903,948-11,904,142 (-)	193	29	Fw: *YGAGGAGTTYGTAGGAGTT Rv: *CATCTCCRCTTTTATTATCTAAAC
CTNND2_L	hg38_chr5:11,904,120-11,904,463 (-)	344	56	Fw: *GGTATTGGGTATGTTYGTATTYGG Rv: *ACRAACTCCTACRAACTCCTCRAA

^s without adapters and barcodes, * amplicons overlap in 2 CpGs, * adapter overhangs: Fw: AAGACTCGGCAGCATCTCCA, Rv: GCGATCGTCACTGTTCTCCA;

Y = C + T, R = A + G

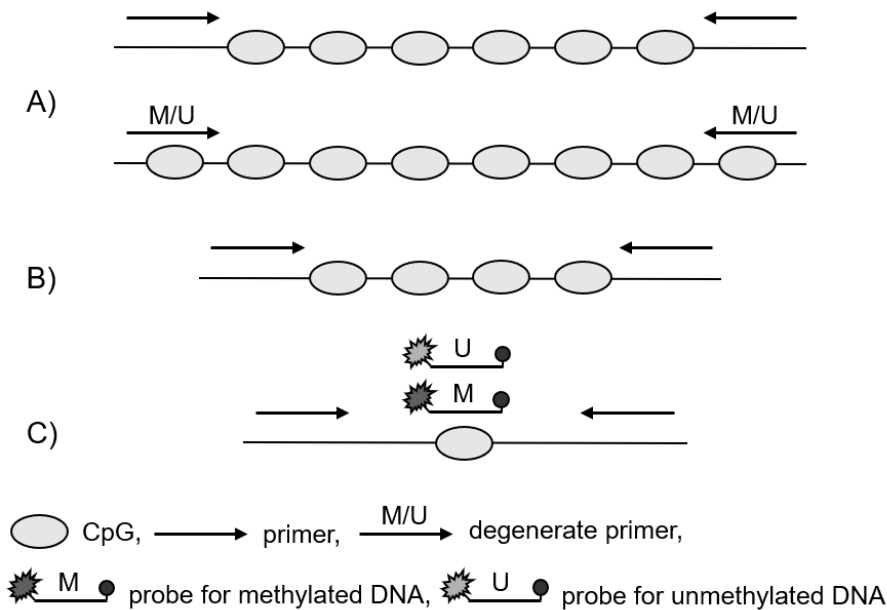


Figure 8 Schematic representation of PCR-based methods used for DNA methylation analysis. A) Next-generation sequencing: the upper scheme shows classical arrangement in bisulfite sequencing using methylation independent (CpG free) primers. In the bottom one, degenerate primers that included CpGs were utilized enabling amplification of both methylated and unmethylated sequence. B) For methylation sensitive high-resolution melting analysis methylation independent primers were used. Methylation status was then determined according melting profiles. C) Duplex real-time PCR assay employed methylation independent primers and TaqMan probe specific for methylated or unmethylated DNA respectively labeled with two different-colored reporter dyes.

Sequencing libraries were prepared using the Multiplicom approach. Optimized first round PCRs were conducted according to the protocols in Tables 5–7. All PCR amplifications were performed in Veriti™ Thermal Cycler (Thermo Fisher Scientific). Bisulfite treated universal methylated and unmethylated DNA (Zymo Research Corporation) were used as controls. PCR products were cleaned using AMPure XP beads on Biomek 4000 (Beckman Coulter, Brea, CA, USA), and verified to be the expected size and free of primer dimers by agarose gel electrophoresis.

Table 5 PCR protocol for first round amplification using AmpliTaq Gold DNA Polymerase

PCR setup		
Component		Volume
PCR grade water		to 20 μ L
10X Reaction Buffer no MgCl ₂		2 μ L
MgCl ₂ (25 mM)		2 μ L
dNTP Mix (2.5 mM)		1.6 μ L
Forward primer (10 μ M)		1 μ L
Reverse primer (10 μ M)		1 μ L
AmpliTaq Gold DNA Polymerase (5 U/ μ L)		0.25 μ L
Template DNA		2 μ L
PCR thermal profile I		
Step	Temperature ($^{\circ}$ C)	Time
Initial denaturation	95	10 minutes
35/40* PCR Cycles	Denature	95
	Anneal	56/59**
	Extend	72
Final Extension	72	5 minutes
Hold	15	Indefinitely
PCR thermal profile II		
Step	Temperature ($^{\circ}$ C)	Time
Initial Denaturation	95	5 minutes
40 PCR cycles	Denature	95
	Anneal	56/57/59/62**
	Extend	72
Final Extension	72	5 minutes
Hold	15	Indefinitely

* 35 cycles apply to CTNNA2_1 and CTNND2_1

** Annealing temperatures: 56 $^{\circ}$ C applies to CTNNA2_1, PCDH10_2 and PCDH17_1; 57 $^{\circ}$ C to CDH10_1, CDH10_2 and CDH13; 59 $^{\circ}$ C to CTNND2_1, CTNND2_2, PCDH8_1, PCDH10_1 and PCDH17_3 and 62 $^{\circ}$ C applies to CDH18_1 and CDH18_2

Table 6 PCR protocol for first round amplification using Platinum *Taq* DNA Polymerase

PCR setup			
Component		Volume	
PCR grade water		to 20 μ L	
10X PCR Buffer, Minus Mg		2 μ L	
MgCl ₂ (25 mM)		1.25 μ L	
dNTP Mix (2.5 mM)		1.5 μ L	
Forward primer (10 μ M)		0.6 μ L	
Reverse primer (10 μ M)		0.6 μ L	
Platinum <i>Taq</i> DNA Polymerase (5 U/ μ L)		0.15 μ L	
Template DNA		2 μ L	
PCR thermal profile			
Step	Temperature ($^{\circ}$ C)		Time
Initial denaturation		95	2 minutes
40 PCR cycles	Denature	95	25 seconds
	Anneal	56/60*	30 seconds
	Extend	72	35 seconds
Final Extension		72	5 minutes
Hold		15	Indefinitely

* Annealing temperatures: 56 $^{\circ}$ C applies to PCDH17_2 and 60 $^{\circ}$ C to PCDH8_2

Table 7 PCR protocol for first round amplification of CTNNA2_2 using High Fidelity Platinum *Taq* DNA Polymerase

PCR setup			
Component		Volume	
PCR grade water		to 20 μ L	
10X High Fidelity PCR Buffer		2 μ L	
MgSO ₄ (50 mM)		0.8 μ L	
dNTP Mix (2.5 mM)		1 μ L	
Forward primer (10 μ M)		1 μ L	
Reverse primer (10 μ M)		1 μ L	
Platinum <i>Taq</i> DNA Polymerase High Fidelity (5 U/ μ L)		0.15 μ L	
Template DNA		2 μ L	
PCR thermal profile			
Step	Temperature ($^{\circ}$ C)		Time
Initial denaturation		94	2 minutes
35 PCR Cycles	Denature	94	15 seconds
	Anneal	56	30 seconds
	Extend	68	30 seconds
Final Extension		68	5 minutes
Hold		15	Indefinitely

Diluted PCR products were then amplified in a subsequent barcoding PCR. Unique DNA sequencing barcodes and specific adapters for Illumina sequencing were incorporated into each sample using MID for the Illumina MiSeq® kit (Multiplicom, Niel, Belgium) with minor modifications. Second round PCR products were separated on 2% agarose gel. Specific products were extracted from gel and purified by the NucleoSpin® Gel and PCR Clean-up kit (Macherey-Nagel, Düren, Germany). Purified sample concentrations were measured on the Qubit® Fluorometer (Thermo Fisher Scientific). Selected samples were analyzed using the Agilent BioAnalyzer DNA1000 chip (Agilent Technologies, Santa Clara, CA, USA). All samples were equimolarly pooled into a library, then quantified using the KAPA library quantification assay (Kapa Biosystems, Wilmington, MA, USA), and the 4 nM library was prepared.

NGS was performed on the MiSeq System (Illumina, San Diego, CA, USA) using Reagent Nano Kits v2 with paired-end reads following the manufacturer's instructions. According to the length of analyzed amplicon, 500 or 300 cycles Reagent Nano Kits were used. Most of the amplicons were up to 400 base pair (bp) in length and required use of 500 cycles kit; 300 cycles kits were used for CTNNA2_1, CTNNA2_2 and CTNND2_S amplicons. Given the fact that these amplicons were less than 200 bp in length, the highly fragmented DNA extracted from FFPE tissue samples could be used for NGS analysis along with DNA from fresh frozen tissue samples.

A final volume of 20% PhiX spike-in control was added to the library to increase sample diversity. The final library was denatured and diluted to 9 pM. The prepared library, along with Multiplicom read 1, read 2 and index primers, was then loaded to the reagent cartridge. Data from MiSeq runs were uploaded to BaseSpace, Illumina's genomics cloud computing environment. Runs generated sequencing data in FASTQ format files.

For analysis of acquired FASTAQ data files from NGS and calculation of methylation status of analyzed CpG sites, NextGENe® software version 2.3.4.5 (Softgenetics, State College, PA, USA) was employed. As reference bisulfite-converted sequences with genomic coordinates specified in Table 4 were used.

For problematic amplicons, alternative pipeline was employed. Sequence data quality was verified using the quality control tool FastQC version 0.11.5 (Andrews, 2010). Genome mapping was performed using the gemBS version 3.2.2 application in original setting (Merkel et al., 2019). The reference sequence was used from the NCBI NG_023544.1 database. The gemBS application has been specifically designed to map bisulfite-converted sequences so the correct position of the nucleotides is maintained even if the cytosines have been converted to uracils during bisulfite modification. The mapped data was then visualized in open source Integrative Genome Viewer (IGV) version 2.4.14 (Robinson et al., 2011) and methylation status was derived from read counts of converted and non-converted cytosines.

The overview of NGS workflow employed in this study is outlined in Figure 9.

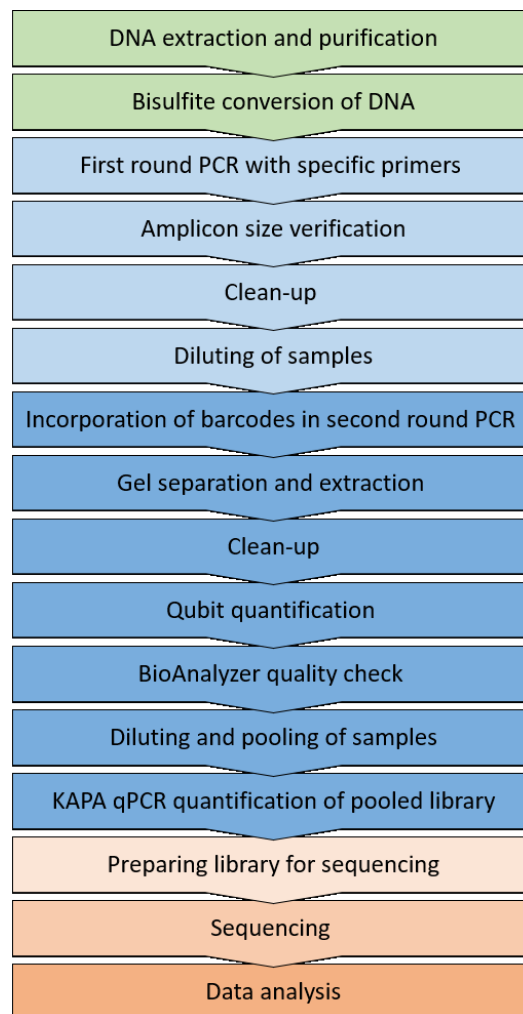


Figure 9 Next-generation sequencing workflow.

3.5 Real-time PCR-based methods for detecting DNA methylation

Based on the results from NGS, CpG sites with the most distinct differences in methylation between tumors and control samples were selected for further analysis. Detected alterations were confirmed on the set of fresh frozen samples from NGS extended by FFPE samples using cost-effective and less demanding or time-consuming methods, such as methylation sensitive high-resolution melting (MS-HRM) analysis or real-time methylation specific PCR.

While conventional PCR techniques detect amplified product in an end-point analysis, mostly by visualization on agarose gel, real-time PCR techniques monitor amplification of product during progress of PCR. It is enabled by including fluorescent molecule in the reaction mixture. Increase in amount of fluorescently labeled DNA then results in proportional increase in the fluorescence signal released during amplification. The fluorescent chemistry used in real-time PCR includes sequence-specific fluorescently labeled probes/primers or non-specific DNA binding dyes. For real-time methylation specific analysis TaqMan probes were used. Non-specific dsDNA binding dyes were employed in MS-HRM experiments.

Primers for bisulfite-converted DNA were designed in on-line platform MethPrimer, considering the fact that FFPE DNA is highly fragmented and also amplicons over 200 bp in length result in lower melting resolution in HRM analysis.

3.5.1 Methylation sensitive high-resolution melting analysis

HRM analysis is an innovative technique based on analysis of melt curves of DNA following real-time PCR amplification. In both steps, PCR and HRM, double-stranded DNA (dsDNA) binding dye is employed. At the beginning of PCR, DNA binding dye is free in solution and exhibits little fluorescence, but after binding to dsDNA its fluorescence significantly increases. Therefore, as the DNA is amplified, the fluorescence signal increases proportionally. In HRM step, the DNA sample with intercalated dye is slowly denatured in consequence of gradually growing temperature. When the dsDNA melts into its single-stranded form, the dye is steadily released, causing change in fluorescence, which is continuously detected by an optical system and melt curve is generated. Sequences that differ in base composition have

different melting profiles. Due to the bisulfite treatment the PCR product originating from the methylated sample has different sequence composition as the PCR product derived from the unmethylated one. It is thus possible to determine methylation status of sample by comparison of its melting profile with profiles specific for methylated and unmethylated control DNAs.

To confirm hypermethylation of selected regions in *CDH13* and *PCDH17* genes, samples were further analyzed using MS-HRM analysis. *CDH13* was divided into two amplicons (*CDH13_a* and *CDH13_b*). Primer sequences along with amplicon length and number of CpG sites per amplicon are summarized in Table 8. Primers did not include any CpGs. Schematic location of primers relative to the investigated CpG sites is depicted in Figure 8B.

Table 8 Amplicon characteristics and primer sequences used in MS-HRM analysis

Amplicon name	Primer sequence 5'-3'	Amplicon size (bp)	CpGs/ Amplicon
CDH13_a	Fw: AGTTTAAAGAAGTAAATGGGATG Rv: AACCAAAACCAATAACTTTACA	130	9
CDH13_b	Fw: TGATTTATTTGGGAAGTTGGT Rv: CCCTCTCCCTACCTAAAACA	189	13
PCDH17	Fw: AAAAGGATTTATAGATTTGTGGTT Rv: AACAAATAAAAAATACATCCCAAAC	144	11

PCR amplification and MS-HRM were performed in Rotor Gene Q (Qiagen, Hilden, Germany) according to the protocol in Table 9. Each run included the no template control, a bisulfite-converted universal methylated and unmethylated DNA (Qiagen) and prepared standard of various methylation percentages (10 %, 25 % and 50 % of universal methylated DNA).

HRM data were analyzed using Rotor Gene Q software 2.3 (Qiagen). Methylation status of each sample was determined by comparing its melting profile with profiles of methylated control, 10% standard which served as a cut-off for methylation status, and unmethylated control.

Table 9 Protocol for MS-HRM analysis of *CDH13* amplicons and *PCDH17*

PCR setup		
Component		Volume
RNase-free water		to 10 μ L
2X EpiTect HRM PCR Master Mix		5 μ L
Forward primer (10 μ M)		0.75 μ L
Reverse primer (10 μ M)		0.75 μ L
Template DNA		2 μ L
PCR thermal profile		
Step	Temperature ($^{\circ}$ C)	
		Time
Initial denaturation		95
		5 minutes
40 PCR cycles	Denature	95
	Anneal	55
	Extend	72
		10 seconds
HRM		55-95; Δ 0.1
		2 seconds
Hold		40
		2 minutes

3.5.2 Real-time methylation specific analysis

In real-time methylation specific PCR, the TaqMan dual-labeled hydrolysis probes were used. TaqMan probes have a fluorescent reporter at 5' end and a quencher of fluorescence at opposite 3' end of the probe. When the quencher is in the proximity to the reporter, it prevents fluorescence emission of the reporter. After the probe hybridize to the DNA during amplification, the 5' to 3' exonuclease activity of the *Taq* polymerase cleaves off the reporter. Free reporter can separate from the quencher and starts to emit fluorescence. As the product targeted by the reporter probe amplifies a proportional increase of fluorescence is emitted. Using of fluorescent probes with different-colored labels in one reaction enables monitoring several target sequences in multiplex PCR.

Duplex real-time PCR assay for measuring DNA methylation was used to analyze two selected CpG sites in the *CDH13*_a amplicon. A set of methylation-independent primers from MS-HRM analysis was used. Probes labeled with two different-colored reporter dyes binding to methylated or unmethylated DNA, respectively, were designed in on-line software Primer3 (Koressaar et Remm, 2007; Untergasser et al. 2012). Sequence of FAM-labeled probe binding to the methylated DNA was 5'-AACCAAACCAATAACTTTACA-3', sequence of HEX-labeled probe

binding to the unmethylated DNA was 5'-TGAGGGAGTGTTAGGAAGGAA-3'. Schematic design of primers and probes relative to the investigated CpG sites is depicted in Figure 8C. PCRs were performed on the Rotor-Gene 6000 5-plex with HRM (Corbett Research, Cambridge, UK) according to the protocol in Table 10.

Reactions were performed in triplicates. Each run included the no template control, a bisulfite-converted universal methylated and unmethylated DNA (Qiagen) and prepared standards of various methylation percentages (10 %, 25 % and 50 % of methylated DNA).

Table 10 PCR protocol for real-time methylation analysis of *CDH13* gene

PCR setup		
Component		Volume
RNase-free water		to 20 μ L
Takara Premix 2X		10 μ L
Forward primer (10 μ M)		0.6 μ L
Reverse primer (10 μ M)		0.6 μ L
Methylated probe FAM (10 μ M)		0.6 μ L
Unmethylated probe HEX (10 μ M)		0.6 μ L
Template DNA		2 μ L
PCR thermal profile		
Step	Temperature ($^{\circ}$ C)	
Initial denaturation	95	30 seconds
40 PCR Cycles	Denature	95
	Anneal	55
	Extend	60
Hold	40	2 minutes

Fluorescence data from real-time methylation specific analysis were analyzed using Rotor-Gene 6000 software. The methylation status of amplicon was determined by calculating methylation index:

$$MI (\%) = 100 / (1 + 2^{(CT_m - CT_u)})$$

CT_m represents Ct value of the reaction with probe binding to the methylated DNA; CT_u is Ct value of the reaction with probe binding to the unmethylated DNA. For amplicon to be considered methylated the value of MI had to be over 5 %. If there was an increase in fluorescence emitted only by HEX-labeled probe, the amplicon was considered unmethylated.

3.6 The Cancer Genome Atlas methylation data

Publicly available dataset containing 302 cases of ovarian serous adenocarcinoma was downloaded from The Cancer Genome Atlas (TCGA) Data Portal. The filter was set for selection of white women of not Hispanic or Latino ethnicity. Cases were staged according to the 1988 FIGO staging system. All cases were classified as G3 (poorly differentiated, i.e. high-grade, $n = 236$), eventually G2 (moderately differentiated, $n = 25$). Data were not available for 41 cases. The majority of tumors were diagnosed at late stages (stage III or IV); only 10 tumors were classified as stage I or II. Stage data were not available for 36 cases. The median age at the time of diagnosis was 60 years (37–87 years).

DNA used for methylation analysis in the TCGA project was extracted from fresh frozen tissue samples of primary tumors. DNA methylation levels were detected in limited number of CpG sites using the Illumina Infinium HumanMethylation27 BeadChip arrays. In each of *CDH10*, *CDH18*, *PCDH8* and *CTNND2* genes, two CpG sites were covered by methylation array, but they did not match any of the CpGs analyzed in our study. In *CTNNA2* gene, 4 CpG sites were analyzed without any match to our CpGs. *PCDH10* gene was not selected for methylation analysis at all. From 9 CpGs analyzed by TCGA project in *CDH13* gene, two CpGs (cg08977371 and cg08747377) were investigated in our study. In *PCDH17* gene, two CpG sites were included in the array and one of them (cg14893163) was analyzed also in our study.

Quantitative measurement of methylation was expressed as beta-value, which is the ratio of the methylated probe intensity and the sum of methylated and unmethylated probe intensities. The cut-off for methylation was set at the same level as in NGS analysis (0.15 %).

3.7 Statistical analysis

Categorical variables were compared by two-tailed Fisher's exact test and/or Chi square test. The Kaplan-Maier method and Logrank test were used to determine overall survival rate and significance. The tests were two tailed and $p < 0.05$ was considered statistically significant. Statistical analyses were performed in data analysis software TIBCO Statistica version 13 (TIBCO Software Inc., Palo Alto, CA, USA).

Following diagnostic parameters were calculated:

$$\text{Sensitivity (\%)} = \text{TP} / (\text{TP} + \text{FN}) * 100$$

$$\text{Specificity (\%)} = \text{TN} / (\text{TN} + \text{FP}) * 100$$

$$\text{Positive predictive value, PPV (\%)} = \text{TP} / (\text{TP} + \text{FP}) * 100$$

$$\text{Negative predictive value, NPV (\%)} = \text{TN} / (\text{TN} + \text{FN}) * 100$$

$$\text{Efficiency (\%)} = (\text{TP} + \text{TN}) / (\text{TN} + \text{TP} + \text{FN} + \text{FP}) * 100$$

where TP means true positives, FN false negatives, TN true negatives and FP false positives.

4 Results

4.1 Next-generation sequencing

Altogether, eleven sequencing runs were needed to analyze all amplicons. All runs had paired-end configuration; for three runs, read length was 2×150 bp (when 300 cycles kit was used), for the rest of runs, it was 2×250 bp (500 cycles kit). The average number of reads per amplicon was 8,600. The percentage of bases with a quality score of 30 or higher ranged from 84.47–96.70 %. Data quality of all runs was very high, so no quality trimming prior aligning was needed. Average percentage of reads uniquely aligned to PhiX genome ranged from 16.05–22.31 % (libraries were spiked with 20% PhiX). Average error rate based on alignment to PhiX was 1.09 %.

Example of the BaseSpace Sequence Hub charts and run metrics is shown in Figure 10.

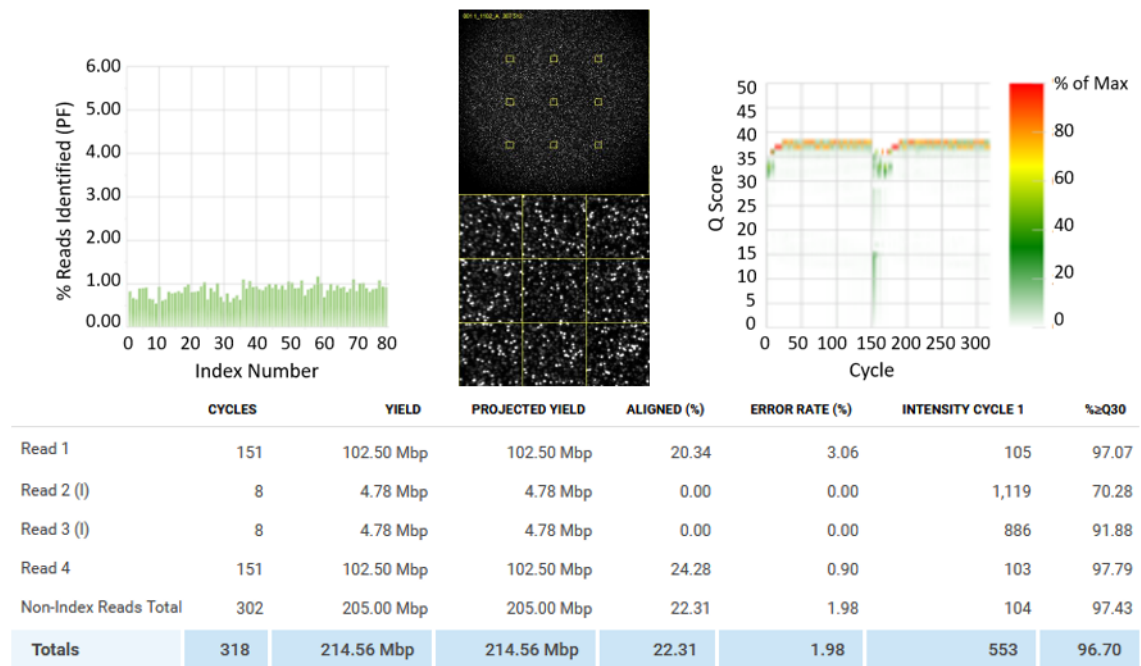


Figure 10 *CTNND2* sequencing run data from BaseSpace Sequence Hub. Indexing QC chart, on the left upper part, displays the total fraction of passing filter reads assigned to each indexed sample. The thumbnail images in the middle show cluster densities. QScore heatmap, on the right, provides an overview of quality scores across cycles. Read metrics table, on the bottom, summarizes overall statistics about the run. QC, quality control.

4.1.1 Cadherins

Selected regions of *CDH10*, *CDH13* and *CDH18* genes were analyzed using NGS. In two of *CDH10* amplicons, 18 CpG sites were examined, single amplicon of *CDH13* covered 23 CpGs, and selected region of *CDH18* was divided into two amplicons containing 28 CpGs altogether.

In all analyzed amplicons, methylation status was examined in 20 fresh frozen samples (10 tumors and 10 control samples). However, some samples had to be excluded from further analysis due to the low coverage. Schematic representation of detected methylation is depicted in Figure 11.

The DNA methylation profile of *CDH10* was compared in 12 samples (6 tumors, 6 control samples). Only sporadic non-significant methylation was detected. Methylation status of *CDH13* was examined in 10 samples (6 tumors, 4 control samples). Methylation was detected in 3 tumor samples; control samples were methylation free. The methylated sites were selected for further analysis to confirm detected methylation. Regions covered by two HRM assays are indicated in Figure 11. Methylation profile of *CDH18* was compared in 14 samples (6 tumors, 8 control samples). CpG3 was methylated in all control samples, whereas there was only one tumor sample with detected methylation at this site. In the remaining 27 analyzed CpGs only sporadic non-significant methylation was present.

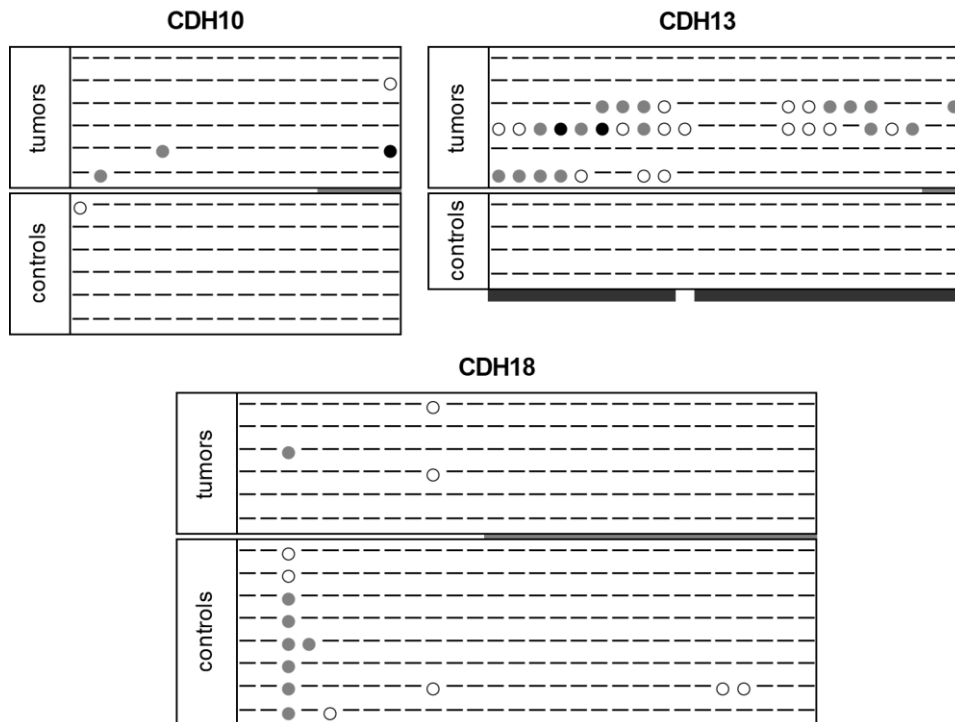


Figure 11 Next-generation sequencing methylation data of cadherins. Each dash represents CpG without methylation (cut-off 15%). Methylated CpGs are displayed as circles: white 15–24.9%, grey 25–49.9%, and black over 50% methylation. Grey band in the middle of each table marks CpGs clustered in CpG island. Black bands at the bottom of the table with *CDH13* methylation data shows the gene regions covered by two HRM assays.

4.1.2 Protocadherins

Methylation status of the *PCDH8*, *PCDH10* and *PCDH17* genes in 20 fresh frozen samples (10 tumors, 10 controls) was examined. Selected region of *PCDH8* was divided into two amplicons containing 43 CpG sites, two amplicons of *PCDH10* covered 22 CpGs and three amplicons of *PCDH17* contained 52 CpGs altogether. Schematic representation of methylation detected in 5 successfully analyzed amplicons (*PCDH8_1*, *PCDH8_2*, *PCDH10_1*, *PCDH17_2* and *PCDH17_3*) shows Figure 12. Analysis of *PCDH10_2* and *PCDH17_1* amplicons was impossible since both analysis tools failed to align sequencing data to the reference sequences.

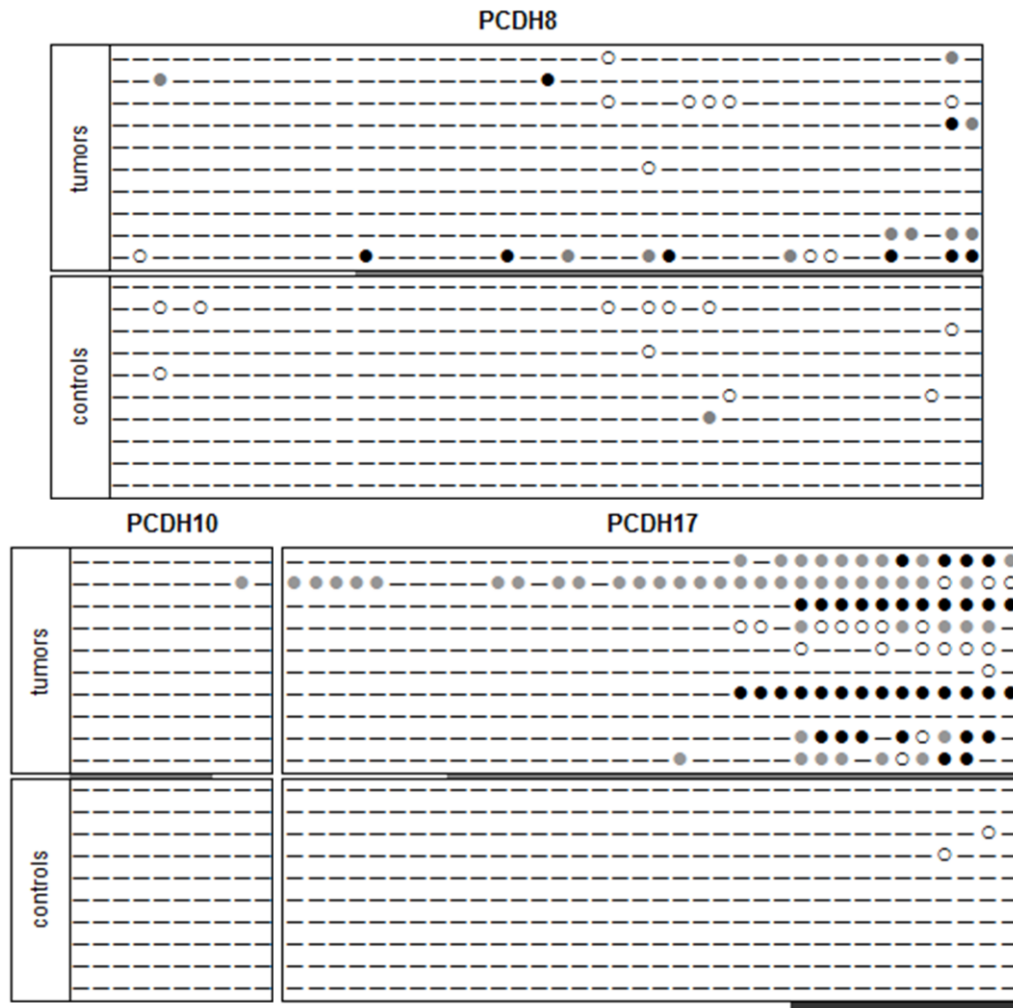


Figure 12 Next-generation sequencing methylation data of protocadherins. Each dash represents CpG without methylation (cut-off 15%). Methylated CpGs are displayed as circles: white 15–24.9%, grey 25–49.9%, and black over 50% methylation. Grey band in the middle of each table marks CpGs clustered in CpG island. Black band at the bottom of the table with *PCDH17* methylation data shows the gene region covered by HRM assay.

PCDH8 amplicons showed only sporadic methylation in both tumors and controls samples. Except one methylated CpG across all samples, there was no methylation detected in 10 analyzed CpGs of *PCDH10_1* amplicon. Statistically significant site-specific methylation was present in 10 of 36 analyzed CpGs in *PCDH17* gene (amplicons *PCDH17_2* and *PCDH17_3*). In this area near the end of analyzed region, high methylation was present in over 60 % of tumor samples, with only minor methylation of one CpG in two control samples. These sites were selected for further analysis by MS-HRM (Figure 12).

4.1.3 Catenins

DNA methylation was analyzed in selected regions of *CTNNA2* and *CTNND2* genes. Two short *CTNNA2* amplicons covered 40 CpG sites. The length of short amplicons was up to 200 bp, enabling NGS methylation analysis of FFPE tissue samples. Therefore, in addition to 20 fresh frozen samples (10 tumors, 10 controls), 18 FFPE samples (10 tumors, 8 controls) were analyzed as well. Only sporadic methylation of few CpGs was detected across all the samples. Schematic presentation of methylation detected in *CTNNA2* gene is depicted in Appendices in Figure A2.1.

Short amplicon *CTNND2_S* covered 29 CpGs. Methylation profile was compared in 20 fresh frozen tissue samples (10 tumors, 10 controls) and 50 FFPE tissue samples (30 tumors, 20 controls). Scattered methylation without any distinguishable pattern was present across all CpGs in 6 tumors and 17 control samples. In two tumor samples, methylation was detected in all of analyzed CpGs. The rest of the samples were methylation free. Methylation detected in short amplicon of *CTNND2* gene is presented in Appendices in Figure A2.2. Amplicon *CTNND2_L* covered 56 CpGs. Methylation profile was compared in 20 fresh frozen samples (10 tumors, 10 controls). Except one tumor and one control sample, no methylation was detected (Appendices, Figure A2.3).

4.2 Confirmation methods

4.2.1 *CDH13* methylation

For confirmation of detected changes in *CDH13* methylation profile, primers for two HRM assays and duplex real-time PCR were designed. First HRM amplicon (*CDH13_a*) covered 9 CpG sites (CpG1–9 from NGS); two of them (CpG7 and 8) were then further analyzed using real-time PCR assay. An example of HRM curves is presented in Figure 13. The second amplicon (*CDH13_b*) covered another 13 CpGs (CpG11–23 from NGS). In the control samples, both of analyzed amplicons in the *CDH13* gene were methylation free. Analysis of the first amplicon showed methylation-positive pattern for 13.1 % (8/61) of tumor samples. Real-time PCR assay further confirmed the level of observed methylation (12.5 % of methylated tumor samples). Methylation detected in the second HRM amplicon was slightly higher, 19.7 % (12/61).

In both of HRM amplicons, methylation was detected more frequently in the early stages (stage I and II), than in the late ones (stage III and IV). The early stage tumors methylation of the first amplicon was observed in 21.4 % cases (3/14), versus 10.6 % (5/47) in the late stage tumors ($p = 0.37$). The second amplicon methylation observed in early stages was 28.6 % (4/14); in the late stages, detected methylation decreased to 17 % (8/47, $p = 0.45$). The decrease in detected methylation was not statistically significant.

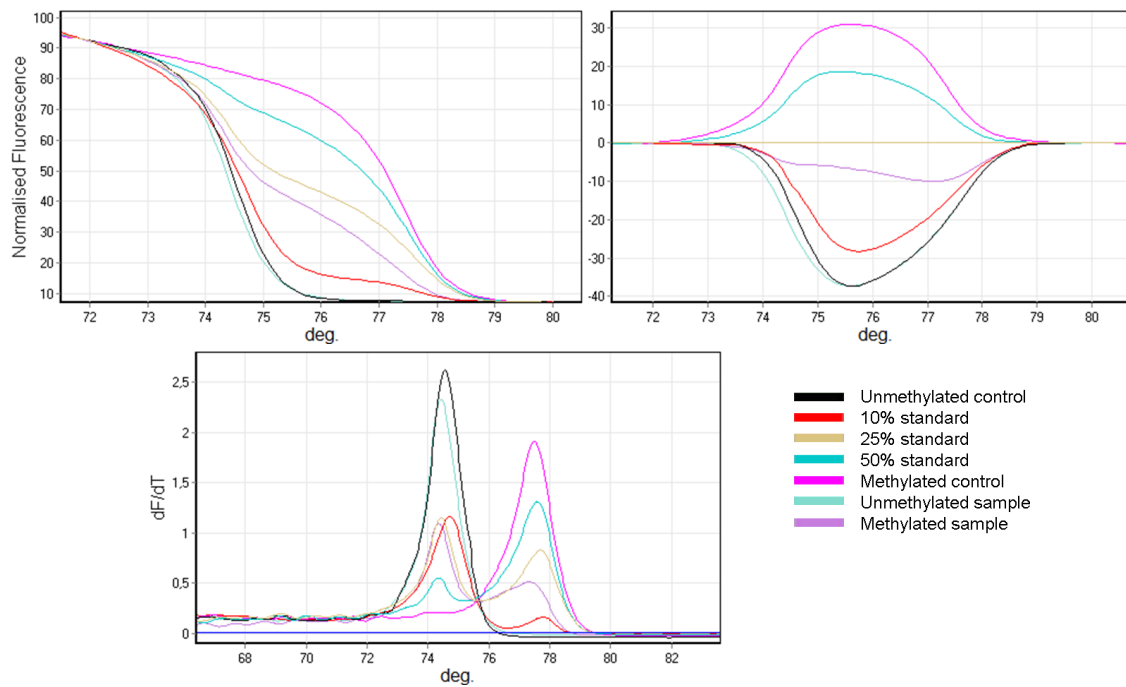


Figure 13 High-resolution melting analysis of CDH13_a amplicon. Normalized graph (top left), difference graph (top right) and melting plots (bottom) shows curves of variously methylated standards and an example of methylated and unmethylated sample.

4.2.2 PCDH17 methylation

To confirm *PCDH17* hypermethylation detected by NGS, 11 CpGs from PCDH17_3 amplicon were analyzed using MS-HRM. Statistically significant methylation-positive pattern ($p < 0.01$) was observed in 60.7 % (37/61) of tumor samples. All of the control samples were methylation free. Methylation was detected with approximately the same frequency in early or late stages tumors, 57.1 % (8/14) of early stage tumors versus 61.7 % (29/47) of late stage ones.

4.3 TCGA methylation data analysis

4.3.1 *CDH13* methylation

The methylation array covered 9 CpG sites from the promoter region of *CDH13* gene. Two of them were investigated also in our project; CpG sites identified as cg08977371 (corresponding to CpG8 from NGS analysis of *CDH13*) and cg08747377 (corresponding to CpG15). In our study, both NGS, as well as real-time PCR-based methods, were used for analysis of these CpG sites.

In TCGA dataset, cg08977371 methylation was detected in 32.1 % (97/302) of cases. NGS analysis of CpG8 showed methylation-positive pattern in three of six tumors. MS-HRM analysis of the amplicon that covered CpG8 revealed methylation in 13.1 % (8/61) of tumor samples. The ratio of methylated samples was much lower, but it can be caused by the fact that HRM assay covered another 8 CpGs. However, real-time PCR assay, that beside CpG8 covered just one more CpG, confirmed the level of the methylation previously detected by HRM.

Methylation of cg08747377 was present in 17.5 % (53/302) of cases in TCGA dataset. Using NGS in our study, methylation at CpG15 was detected in two of six tumor samples. MS-HRM analysis of larger set of samples showed methylation-positive pattern in 19.7 % (12/61) of cases. In spite of another 12 CpG sites (beside CpG15) covered by HRM assay, the detected methylation does not differ from the methylation observed in TCGA project.

4.3.2 *PCDH7* methylation

Two CpG sites in the promoter region of *PCDH17* gene were covered by the methylation array in TCGA project. CpG site identified as cg14893163 corresponded to the second CpG of *PCDH17_2* amplicon in our study. This CpG was analyzed using NGS only and was not selected for further analysis. Methylation of cg14893163 was detected in 6.6 % (20/302) of cases. Using NGS, methylation at this site was detected only in one of ten tumor samples. The analysis of TCGA data confirmed methylation status of this CpG site detected in our study.

4.4 Follow-up

The patients were followed up in January 2019 and data for the overall survival (OS) and the disease-free survival (DFS) calculation were collected from patients. It was impossible to obtain complete data of 15 patients, as they were subsequently treated in another health care facility or refused to undergo further treatment. During the follow-up period, 27 patients (58.7 %, 27/46) died due to HGSOC, 17 of them (37.0 %, 17/46) within 5 years. Eleven patients (18.6 %, 11/59) had persistent disease or the disease progressed during the treatment. Relapse occurred in 27 patients (58.7 %, 27/46). OS of patients ranged from 2–216 months, with a median of 52 months; median DSF was 18 months. At the end of the follow-up period, 19 patients (41.3 %, 19/46) were still alive, 11 of them (23.9 %, 11/46) in complete remission without any relapse. Survival data of all patients along with detected methylation are summarized in Appendices.

The Kaplan-Maier analysis and Logrank tests were used to determine overall survival rate and significance. Kaplan-Meier survival plots for *CDH13* and *PCDH17* genes respectively are depicted in Figure 14 and Figure 15. Although overall survival was slightly better in the group of patients where no methylation was observed, the correlation between gene methylation and survival data was not considered statistically significant.

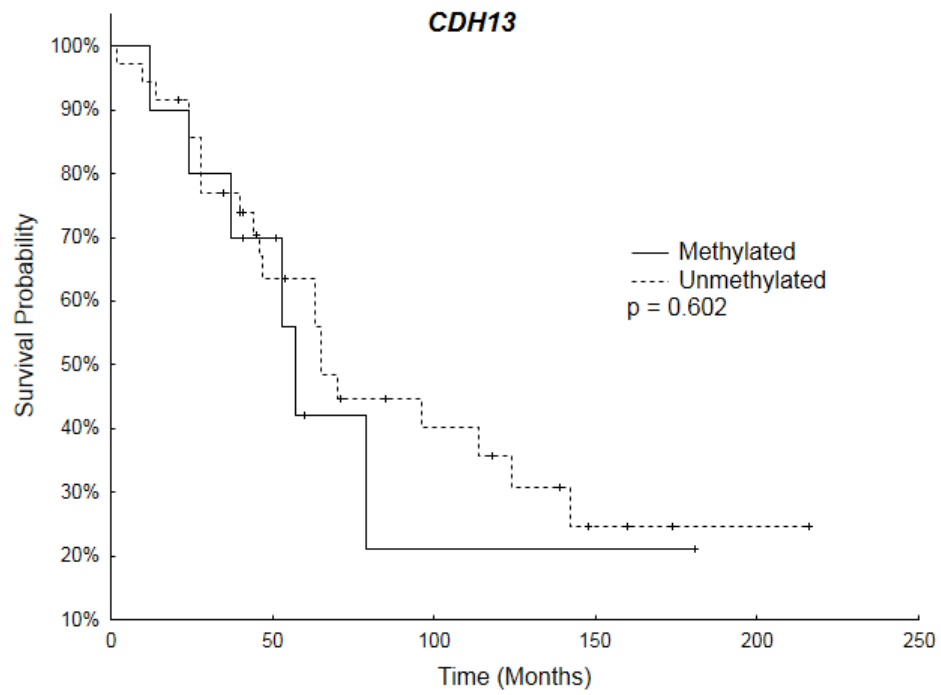


Figure 14 Kaplan-Meier survival curves according to the methylation of *CDH13* gene.

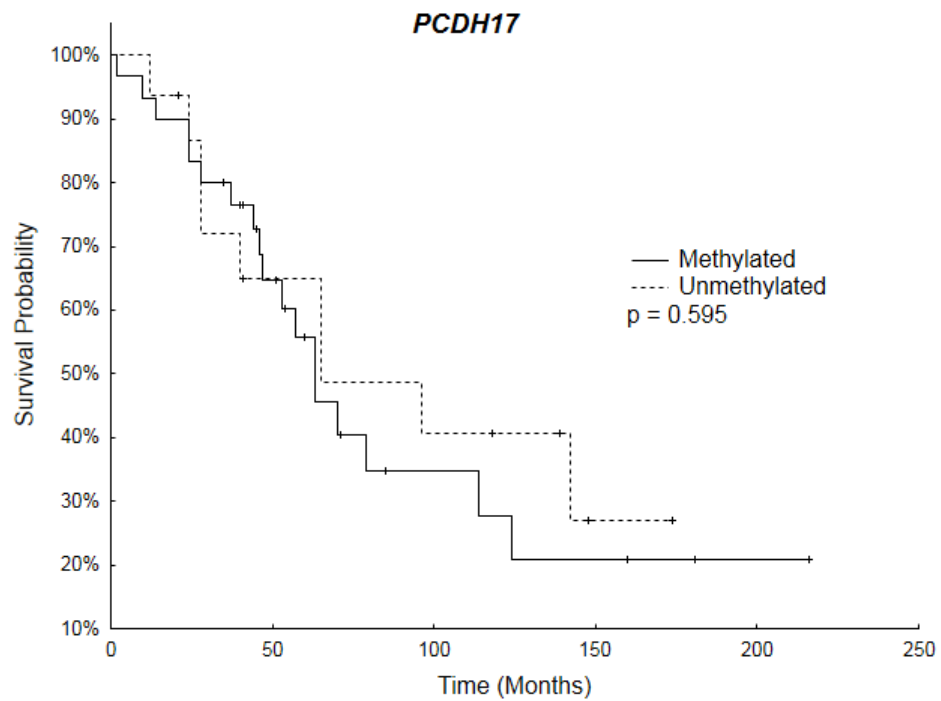


Figure 15 Kaplan-Meier survival curves according to the methylation of *PCDH17* gene.

4.5 DNA methylation panel

The possibility of a methylation panel design was assessed. DNA methylation of selected regions of *CDH13* and *PCDH17* genes was detected in 19.7 % (12/61) and 60.7 % (37/61) of patients, respectively. By evaluating both genes together the detected methylation increased by 4.9 %, to 65.6 % (40/61) of patients.

In order to increase the percentage of patients with detected methylation, another two genes from our previous study were evaluated as possible candidates for methylation panel. Given the fact that *GATA4* and *HNF1B* are transcription factors and thus do not belong to the adhesion molecules that are discussed in this study, they were included in Appendix. Generally, the methylation analysis of *GATA4* and *HNF1B* genes followed the same procedures as described for adhesion molecules. The specific data, such as primer sequences, PCR protocols and thermal profiles, are summarized in Appendix A4. Schematic representation of methylation detected using NGS is depicted in Figure A4.1. The concise description of methylation detected using confirmation methods is part of Appendix A4, as well.

In case of *GATA4* gene, methylation was detected in 31.2 % (19/61) of patients. Selected region of *HNF1B* gene was methylated in 50.8 % (31/61) of patients. Due to the higher percentage of detected methylation, the *HNF1B* gene was assessed first. The involvement of the *HNF1B* gene in the examined methylation panel increased detected methylation by 18 %, to 83.6 % (51/61) of patients. The further addition of the *GATA4* gene to the already tested *CDH13*, *PCDH17* and *HNF1B* led to the increase by another 4.9 %, to 88.5 % (54/61) of patients with detected methylation.

Besides sensitivity, the specificity, PPV, NPV, and efficiency of all the above-mentioned gene combinations were calculated. The diagnostic parameters are summarized in Table 11. The efficiency of four-gene panel reached 94.2 %; NPV was 86 %. Since the analyzed CpGs were selected in the regions without any methylation present in control samples, the specificity and PPV achieved 100% rates.

Table 11 Diagnostic parameters of analyzed genes, included in DNA methylation panel

Gene	Sensitivity (%)	Specificity (%)	PPV (%)	NPV (%)	Efficiency (%)
CDH13	19.7	100	100	46.7	52.9
PCDH17	60.7	100	100	64.2	76.9
CDH13 + PCDH17	65.6	100	100	67.2	79.8
HNF1B	50.8	100	100	58.9	71.2
CDH13 + PCDH17 + HNF1B	83.6	100	100	81.1	90.4
GATA4	31.1	100	100	50.6	59.6
CDH13 + PCDH17 + HNF1B + GATA4	88.5	100	100	86	93.3

PPV, positive predictive value; NPV, negative predictive value.

5 Discussion

High-grade serous ovarian cancer is the most frequent and aggressive form of OC. Just like any other malignancy, it is the consequence of the progressive genetic and epigenetic alterations. These alterations may influence diverse genes involved in the crucial signaling pathways, where cell adhesion molecules play important role. A major class of cell adhesion molecules that mediate cell-to-cell adhesion is the cadherin superfamily. Specific signaling pathways activated by cell-cell interactions are regulated by cadherin-catenin complexes. DNA methylation associated with decreased expression of the cadherin and catenin genes may lead to disruption of cell-cell connections and results thus in epithelial tumor aggressiveness, invasion and metastasis (Cavallaro et Christofori, 2004). In our project, the methylation pattern of selected cadherin and catenin genes was analyzed, with the aim of determining, whether they can serve as potential epigenetic biomarkers of clinical benefit in HGSOc screening, diagnosis, and prognosis. For this purpose, innovative approach was employed. It included use of targeted amplicon NGS as the initial method for selecting the most significant CpG sites. The used technique provided a comprehensive view of methylation patterns in the promoter region and part of the first exon of the analyzed genes. These regions were up to 400 bp in length and covered numerous CpG sites. Considering the fact that NGS is time consuming, labor intensive and expensive method, and requires DNA of high quality, purity and integrity, it was used just for preliminary analysis of selected set of samples. Only DNA extracted from fresh frozen tissue met the quality criteria for analysis of amplicons over 200 bp in length. For analysis of the shorter amplicons, DNA from FFPE tissue samples could have been used as well. CpG sites with the most distinct differences in methylation between tumors and control samples were then analyzed in the whole set of samples using less-demanding methods, such as MS-HRM analysis or real-time methylation specific PCR. The detected methylation was then compared to public available methylation data from TCGA project. The program, supervised by the National Institutes of Health (United States government agency), aims to catalogue the molecular aberrations in various type of cancer for better understanding of genetic and epigenetic basis of cancer that would improve cancer diagnostic, therapy and prevention. Ovarian serous carcinoma was among the cancers selected for study by TCGA.

Due to the lack of any specific symptoms in the early stages, highly invasive HGSOc is mostly diagnosed after the disease has metastasized beyond the ovary. Metastatic spread is promoted by EMT and cadherins, whose main function is cell-to-cell adhesion, are key participants in this process. Epigenetic mechanisms are involved in regulation of cadherin genes participating in EMT. DNA methylation in E-cadherin has been implicated in the initiation and completion of EMT (Strathdee, 2002). Furthermore, various epigenetic modifiers, such as DNMTs, histone deacetylases, methyltransferase and demethylase, are involved in the transcriptional regulation of E-cadherin (Lee et Kong, 2016). The role of E-cadherin gene promoter methylation in OC has been previously investigated (Montavon et al., 2012; Wang et al., 2016).

Our project focused on methylation analysis of genes encoding unconventional cadherins (*CDH10*, *CDH13* and *CDH18*), little studied $\delta 2$ group of non-clustered protocadherins (*PCDH8*, *PCDH10* and *PCDH17*), and cadherin-associated proteins, catenins (*CTNNA2* and *CTNND2*).

CDH10 gene (also known as *T2-Cadherin*) is predominantly expressed in central nervous system. It also can be found in epithelial cells of prostate, in testes, ovary, placenta, kidney and small intestine (Stelzer et al, 2016). *CDH10* plays a key role in prostate epithelial differentiation and it is downregulated in prostate cancer (Walker et al., 2008). Mutations of this gene were associated with gastric and colorectal cancer (An et al., 2015) and lung squamous cell carcinoma (Li et al., 2015). According to our knowledge, this is the first study evaluating *CDH10* methylation in OC. Preliminary scan showed only sporadic non-significant methylation, indicating that methylation of selected region is not associated with ovarian carcinogenesis.

The protein encoded by *CDH13* gene (also known as *T-Cadherin*, *H-Cadherin*, *CDHH* or *P105*) acts as a negative regulator of axon growth during neural differentiation. When expressed on vascular endothelial cells it promotes angiogenesis, on stromal cells it inhibits neovascularization (Stelzer et al, 2016). Downregulation of *CDH13* in cancer cells and upregulation on the vasculature of various tumors negatively regulates tumor cell proliferation and angiogenesis, but at the same time, it also enhances tumor progression (Andreeva et Kutuzov, 2010). The gene is hypermethylated in many types of cancer including OC (Bol et al., 2010). To the best of our knowledge, our study is the first one to investigate methylation status of *CDH13*

in HGSOC using NGS. Preliminary NGS scan showed methylation in 3 of 6 tumor samples, whereas the control samples were methylation free. Further MS-HRM analysis revealed methylation-positive pattern in 13.1 % (8/61) and 19.7 % (12/61) of tumor samples (in the first and second HRM amplicon, respectively). The level of methylation observed in the first amplicon was further confirmed by real-time PCR assay (12.5 % of methylated tumor samples). There was no methylation detected in the control samples using confirmation methods. The lower presence of methylation detected by HRM assays could be caused by the assay design. The sample is observed as methylated only if most of the included CpGs are methylated (the first HRM amplicon covered 9 CpG sites, the second one 13 CpGs). The small number of samples analyzed by NGS probably also played a role in disproportional high percentage of the detected methylation. Previous studies analyzed *CDH13* methylation using MS-MLPA or MSP that can focus only on a few CpG sites. They reported statistically non-significant methylation in OC samples compared with normal/benign tissue (Feng et al. 2008) or very low methylation in tumors (Rathi et al., 2002). Bol et al. (2010) detected methylation in 16.0 % of BRCA1-related tumors and in 21.5 % of control sporadic OC. Chmelarova et al. (2012) reported methylation in more than 50 % of OC. The disparity between detected methylation is most likely caused by analysis of distinct CpG sites. Moreover, all above mentioned studies investigated overall methylation in various subtypes of OC (they did not focus specifically on HGSOC) and different distribution of OC subtypes in each study group could affect results as well.

Our results were compared to the public available methylation data from TCGA program, specifically from the project focused on serous ovarian adenocarcinoma. Of 9 CpG sites in the *CDH13* gene covered by their methylation array, two CpGs were investigated also in our study using both NGS and confirmation methods as well. In cg08977371 from TCGA dataset methylation was detected in 32.1 % (97/302) of cases. Corresponding CpG in our study was methylated in three of six tumors, as detected by NGS, and further MS-HRM analysis revealed methylation in 13.1 % (8/61) of tumor samples. The discrepancy between TCGA and our data most likely results from different techniques used for detection of methylation. Moreover, our HRM assay covered additional 8 CpGs, methylation of which could affect the methylation status of concerned CpG site. Methylation of the second CpG, identified as cg08747377, was present in 17.5 % (53/302) of cases in TCGA dataset. Using NGS in our study, methylation of corresponding CpG site was detected in two of six tumor

samples. MS-HRM analysis of larger set of samples showed methylation-positive pattern in 19.7 % (12/61) of cases. The methylation detected at this site of the *CDH13* gene is approximately at the same level as the methylation observed in TCGA project.

In subsequent analysis of the follow-up data of patients, correlation between detected methylation in the *CDH13* gene and survival data was investigated. Although, overall survival was slightly better in the group of patients where no methylation was observed, the difference from the group with detected methylation was not considered statistically significant. The analyzed regions of the *CDH13* gene were thus not considered suitable for further examination as prognostic marker.

CDH18 (also known as *CDH14*, *CDH24* or *Ey-Cadherin*) is expressed in the central nervous system and its role as tumor-suppressor gene has been recently demonstrated in brain cancer (Bai et al., 2018). Copy number variants of *CDH18* gene have been associated with familial and early-onset colorectal cancer (Venkatachalam et al., 2011) and deletions in this gene have been found in odontogenic tumors (Heikinheimo et al., 2007). According to our knowledge, there have not been any published studies focused on the *CDH18* methylation in association with cancer. In our study, methylation profile of 28 examined CpGs in the *CDH18* gene showed weak scattered methylation, except for one CpG where methylation was present in all control samples. Due to the fact that methylation at this site was detected also in a tumor sample; the gene was not selected for further analysis. However, the loss of methylation in the tumor samples suggests possible role of *CDH18* in HGSOC progression.

PCDH8 gene (also known as *Arcadlin* or *PAPC*) encodes an integral membrane protein that takes part in cell adhesion in central nervous system and may play a role in down-regulation of dendritic spines (Stelzer et al, 2016). It is considered to function as a tumor suppressor in hypopharyngeal carcinoma (Li et al., 2018). Low expression of *PCDH8* is thought to promote OC progression (Cao et al., 2018). Hypermethylation of the *PCDH8* gene has been associated with prostate cancer (Lin et al., 2014) or bladder cancer (Niu et al., 2014). Although different studies have confirmed the significance of altered methylation of *PCDH8* in other types of cancers, there is no evidence of its hypermethylation being associated with OC. In this study, however, using NGS as preliminary method for investigating methylation status, only sporadic methylation was observed in the selected region of *PCDH8*.

The protein encoded by the *PCDH10* gene (also known as *PCDH19*, *OL-PCDH* or *KIAA1400*) is a neuronal receptor involved in specific cell-cell connections in the brain. This gene plays a role in inhibiting cancer cell motility and cell migration (Stelzer et al, 2016). The prognostic value of *PCDH10* promoter methylation has been suggested in different types of cancer, such as prostate cancer (Deng et al., 2016) or gastric cancer (Hou et al., 2015). According to our knowledge, this is the first study evaluating *PCDH10* methylation in OC. There was no methylation detected in 10 analyzed CpGs of *PCDH10* gene, indicating that methylation of these sites is not involved in HGSOC development and progression.

Similar to the other members of $\delta 2$ subfamily of protocadherins, *PCDH17* (also known as *PCDH68*) is widely expressed in the nervous system and involved in axon development or function (Stelzer et al, 2016). The importance of altered *PCDH17* methylation has been confirmed in various types of cancers, such as bladder cancer (Luo et al., 2014) or breast cancer (Yin et al., 2016). The association of altered methylation in *PCDH17* gene with OC has not been previously investigated. In our study, methylation-positive pattern was observed in 60.7 % (37/61) of the tumor samples, whereas all the control samples were methylation free. Our findings suggest that methylation of *PCDH17* gene may play an important role in HGSOC.

Since molecular markers of early stage HGSOC are critically needed, the possibility of using *PCDH17* methylation for early detection was investigated. For this purpose, the patient samples were divided into two groups: early stage tumors (stage I and II) and late stage tumors (stage III and IV). Methylation of the *PCDH17* gene was observed with approximately the same frequency in both groups, 57.1 % (8/14) versus 61.7 % (29/47). Even if there was only little difference between the early and late stage tumors, the mere fact that the *PCDH17* methylation could be detected in the early stages, suggests its potential for further examination as a part of biomarker panel for early detection.

The correlation between methylation detected in the *PCDH17* gene and survival data of patients was then investigated. However, the presence of *PCDH17* methylation was not associated with overall survival of patients, suggesting that selected CpG sites are unsuitable for further examination as prognostic marker.

Methylation array in the TCGA project focused on HGSOC investigated methylation status of two CpG sites in the promoter region of the *PCDH17* gene. One

of these CpGs (cg14893163) was also analyzed in our study using NGS as preliminary scan. TCGA project revealed methylation at this site in 6.6 % (20/302) of cases. In our study, methylation at corresponding site was observed only in one of ten tumor samples, so our data were in correlation with those from TCGA project. The second CpG analyzed by TCGA in the *PCDH17* gene promoter showed methylation-positive pattern even in less cases. Based on these findings, *PCDH17* gene could be abandoned as non-significant in terms of methylation in OC. However, in another part of the *PCDH17* gene promoter region our results showed significant methylation in over 60 % of tumor samples. Considering the fact that methylation is site-specific, the proper selection of the most relevant gene region is crucial in methylation analysis. The importance of the location of CpG hypermethylation in relation to gene expression and development of cancer biomarkers has been in detail discussed by Vlodrop et al. (2011) and Koch et al. (2018).

Catenins are intracellular proteins found in complexes with cadherins that connect cadherins to the cell's cytoskeleton. They are frequently downregulated during EMT and have been associated with metastatic process (Bukholm et al., 1998). *CTNNA2* (also known as *alpha-2-catenin*, *alpha-N-catenin*, *CAPR*) has been implicated as a linker between cadherin adhesion receptors and the cytoskeleton of the nervous system cells. Beside brain, it is also expressed in testis (Stelzer et al, 2016). It functions as the tumor suppressor gene frequently mutated in laryngeal carcinomas (Fanjul-Fernandez et al., 2013). Single nucleotide polymorphism in *CTNNA2* has been associated with breast cancer susceptibility (Haryono et al., 2015). To the best of our knowledge, our study is the first one to evaluate methylation status of *CTNNA2* in OC. In our study, only sporadic methylation of few CpGs in the *CTNNA2* gene was detected across all the samples, indicating that the methylation of selected region does not play an important role in HGSOC development and progression.

CTNND2 (also known as *delta-2-catenin*, *NPRAP*, *GT24* or *Neurojungin*) has been implicated in brain and eye development. The protein encoded by this gene promotes the disruption of E-cadherin based adherens junction enabling thus cell spreading (Stelzer et al, 2016). Overexpression of *CTNND2* gene associated with decreased expression of tumor suppressor E-cadherin has been confirmed in prostate cancer (Kim, H et al., 2012) and lung adenocarcinomas (Huang et al., 2018). According to our knowledge, this is the first study evaluating methylation

of the *CTNND2* gene in HGSOC. Although extensive region (covering 85 CpG sites) in the promoter and first exon of the *CTNND2* gene was examined in our study, no distinguishable methylation pattern was detected.

Because epigenetic alterations occur early in the cancer development, they provide great potential to serve as biomarkers for screening and early detection. Currently, 14 methylation-based biomarker assays are commercially available indicated respectively in prostate, bladder, lung and colorectal cancer, and in prediction of response to temozolomide in glioblastoma (Koch et al., 2018). Assay for simultaneous detection of methylation in *NDRG4* and *BMP3* genes, and two different *SEPT9* methylation assays for early detection of colorectal cancer have been approved by FDA (Food and Drug Administration). Numerous studies investigated methylation of various genes in effort to find an effective screening test or early detection biomarkers in highly aggressive and metastatic OC. So far, all examined genes lacked sufficient combination of specificity and sensitivity to become the reliable biomarkers. To increase sensitivity and specificity of potential biomarkers, different combinations of several genes have also been investigated. Hentze et al. (2019) summarized up-to-date results of research investigating the potential of DNA methylation-based biomarkers in OC, without considering individual subtypes of OC though. Montavon et al. (2012) focused their research just on HGSOC and found that combination of the methylation status of *HOXA9* and *ENI* genes could discriminate HGSOC from benign ovarian surface epithelium with a sensitivity of 98.8 % and a specificity of 91.7 %. However, further studies using a larger cohort are needed to confirm these results.

In our study, the possibility of designing a methylation panel covering more genes was assessed, as well. Altogether, of the eight genes that underwent the initial examination using NGS, only *CDH13* and *PCDH17* showed significant methylation-positive pattern in the tumor samples and were thus selected for further investigation. As mentioned above, the methylation frequency of the *CDH13* and *PCDH17* genes examined individually was 19.7 % (12/61) and 60.7 % (37/61), respectively. Between the two of the genes, *CDH13* with its much lower percentage of detected methylation does not appear to be useful for next consideration as potential biomarker. However, as there were some patients with the methylation present only in *CDH13*, and not in *PCDH17*, the evaluation of both genes together revealed increase in detected

methylation to 65.6 % (40/61) of the patients. In order to further increase number of patients with detected methylation, other candidate genes from our previous studies were investigated. By involving *HNF1B* and *GATA4*, with individually detected methylation in 50.8 % (31/61) and 31.2 % (19/61) of tumor samples, the total number of patients with detected methylation reached 88.5 % (54/61). This increase in sensitivity shows the potential of selected gene regions to be included into a DNA methylation biomarker panel. The efficiency of this four-gene panel was 94.2 %, negative predictive value reached 86 %, and since the primers for confirming analysis were deliberately designed flanking the sites without any methylation in the control samples, the specificity and positive predictive value were both 100 %.

6 Conclusions

In our project, the methylation pattern of selected genes encoding adhesion molecules was investigated in order to evaluate their potential as epigenetic biomarkers of clinical benefit in HGSOc screening, diagnosis, and prognosis.

1. The first objective specified in this project was optimization of NGS method for monitoring DNA methylation. Methodology for 14 amplicons in 8 genes (*CDH10*, *CDH13*, *CDH18*, *PCDH8*, *PCDH10*, *PCDH17*, *CTNNA2*, and *CTNND2*) was successfully optimized. The genes with most distinct alterations in methylation status were then selected for further analysis.
2. In the next step, following the second objective, MS-HRM and real-time methylation specific PCR were optimized to confirm hypermethylation detected in *CDH13* and *PCDH17* gene.
3. MS-HRM analysis of *CDH13* gene showed methylation-positive pattern in 13.1–19.7 % of the tumor samples. The level of methylation observed in the first amplicon was further confirmed by real-time PCR assay. MS-HRM analysis of the *PCDH17* gene revealed methylation-positive pattern in 60.7 % of the tumor samples. All of the control samples were devoid of methylation in both of analyzed genes.
4. As required by the last objective of our project the correlation between detected methylation and clinicopathological characteristics and between methylation and follow-up data of patients was investigated.

CDH13 methylation was detected more frequently in the early stage tumors than in the late stage ones by approximately 10 %. Methylation of the *PCDH17* gene was observed with approximately the same frequency in the early stage tumors as in the late stage ones. Despite the lack of statistically significant differences between stages, the fact that the methylation of the *CDH13* and *PCDH17* genes could be detected in early stages suggests their potential for further examination as a part of biomarker panel for early detection, especially if their methylation could be detected in plasma.

There was no statistically significant correlation observed between methylation of *CDH13* or *PCDH17* and follow-up data of patients. The analyzed genes did not prove potential as prognostic markers.

5. The combined evaluation of *CDH13* and *PCDH17* genes increased the percentage of tumor samples with methylation positive pattern at least in one of the genes to 65.6 %. Further increase in the number of HGSOC patients with detected methylation was observed when another two genes from our previous study were involved. By methylation analysis of the four-gene panel, including *CDH13*, *PCDH17*, *GATA4* and *HNF1B*, the methylation could be detected in 88.5 % of tumor samples. These results indicate that examined genes deserve consideration for further testing in clinical molecular diagnosis of HGSOC.

Our findings indicate that methylation of the *CDH13* and *PCDH17* genes could play an important role in development and progression of HGSOC. With the right selection of the most relevant sites for methylation analysis these genes showed potential to become a target in searching for new clinical epigenetic biomarkers. However, further studies on more extensive group of patients are needed to confirm our novel results.

References

- AHUJA, N., A. R. SHARMA and S. B. BAYLIN (2016) Epigenetic Therapeutics: A New Weapon in the War Against Cancer. *Annu Rev Med*, 67, 73-89.
- ALLEMANI, C., T. MATSUDA, V. DI CARLO, R. HAREWOOD, et al. (2018) Global surveillance of trends in cancer survival 2000-14 (CONCORD-3): analysis of individual records for 37 513 025 patients diagnosed with one of 18 cancers from 322 population-based registries in 71 countries. *Lancet*, 391(10125), 1023-1075.
- AN, C. H., E. M. JE, N. J. YOO and S. H. LEE (2015) Frameshift mutations of cadherin genes DCHS2, CDH10 and CDH24 genes in gastric and colorectal cancers with high microsatellite instability. *Pathol Oncol Res*, 21(1), 181-185.
- ANDREEVA, A. V. and M. A. KUTUZOV (2010) Cadherin 13 in cancer. *Genes Chromosomes Cancer*, 49(9), 775-790.
- ANDREWS S. (2010). FastQC: a quality control tool for high throughput sequence data. Available online at <http://www.bioinformatics.babraham.ac.uk/projects/fastqc>.
- ANGST, B. D., C. MARCOZZI and A. I. MAGEE (2001) The cadherin superfamily: diversity in form and function. *J Cell Sci*, 114(4), 629-641.
- ASIAF, A., S. T. AHMAD, S. A. AZIZ, A. A. MALIK, et al. (2014) Loss of expression and aberrant methylation of the CDH1 (E-cadherin) gene in breast cancer patients from Kashmir. *Asian Pac J Cancer Prev*, 15(15), 6397-6403.
- BAI, Y. H., Y. B. ZHAN, B. YU, W. W. WANG, et al. (2018) A Novel Tumor-Suppressor, CDH18, Inhibits Glioma Cell Invasiveness Via UQCRC2 and Correlates with the Prognosis of Glioma Patients. *Cell Physiol Biochem*, 48(4), 1755-1770.
- BALL, M. P., J. B. LI, Y. GAO, J. H. LEE, et al. (2009) Targeted and genome-scale strategies reveal gene-body methylation signatures in human cells. *Nat Biotechnol*, 27(4), 361-368.
- BALMAÑA, J., O. DÍEZ, M. CASTIGLIONE and O. B. O. T. E. G. W. GROUP (2009) BRCA in breast cancer: ESMO Clinical Recommendations. *Annals of Oncology*, 20(suppl_4), iv19-iv20.
- BANNISTER, A. J. and T. KOUZARIDES (2011) Regulation of chromatin by histone modifications. *Cell Res*, 21(3), 381-395.
- BARTEL, D. P. (2004) MicroRNAs: genomics, biogenesis, mechanism, and function. *Cell*, 116(2), 281-297.
- BARTON, C. A., N. F. HACKER, S. J. CLARK and P. M. O'BRIEN (2008) DNA methylation changes in ovarian cancer: implications for early diagnosis, prognosis and treatment. *Gynecol Oncol*, 109(1), 129-139.
- BAUMER, A., U. WIEDEMANN, M. HERGERSBERG and A. SCHINZEL (2001) A novel MSP/DHPLC method for the investigation of the methylation status of imprinted genes enables the molecular detection of low cell mosaicisms. *Hum Mutat*, 17(5), 423-430.
- BEREK, J. S., S. T. KEHOE, L. KUMAR and M. FRIEDLANDER (2018) Cancer of the ovary, fallopian tube, and peritoneum. *Int J Gynaecol Obstet*, 143 Suppl 2, 59-78.

- BHATLA, N. and A. JONES (2018) The World Ovarian Cancer Coalition Atlas 2018. Available at: <https://worldovariancancercoalition.org/wp-content/uploads/2018/10/THE-WORLD-OVARIAN-CANCER-COALITION-ATLAS-2018.pdf>
- BIBIKOVA, M., Z. LIN, L. ZHOU, E. CHUDIN, et al. (2006) High-throughput DNA methylation profiling using universal bead arrays. *Genome Res*, 16(3), 383-393.
- BOL, G. M., K. P. SUIJKERBUIJK, J. BART, M. VOOIJS, et al. (2010) Methylation profiles of hereditary and sporadic ovarian cancer. *Histopathology*, 57(3), 363-370.
- BONANNO, C., E. SHEHI, D. ADLERSTEIN and G. M. MAKRIGIORGOS (2007) MS-FLAG, a novel real-time signal generation method for methylation-specific PCR. *Clin Chem*, 53(12), 2119-2127.
- BRAICU, O.-L., L. BUDISAN, R. BUIGA, A. JURJ, et al. (2017) miRNA expression profiling in formalin-fixed paraffin-embedded endometriosis and ovarian cancer samples. *OncoTargets and Therapy*, 10, 4225-4238.
- BRUNNER, A. L., D. S. JOHNSON, S. W. KIM, A. VALOUEV, et al. (2009) Distinct DNA methylation patterns characterize differentiated human embryonic stem cells and developing human fetal liver. *Genome Res*, 19(6), 1044-1056.
- BUKHOLM, I. K., J. M. NESLAND, R. KARESEN, U. JACOBSEN, et al. (1998) E-cadherin and alpha-, beta-, and gamma-catenin protein expression in relation to metastasis in human breast carcinoma. *J Pathol*, 185(3), 262-266.
- CALURA, E., R. FRUSCIO, L. PARACCHINI, E. BIGNOTTI, et al. (2013) MiRNA landscape in stage I epithelial ovarian cancer defines the histotype specificities. *Clin Cancer Res*, 19(15), 4114-4123.
- Cancer Genome Atlas Research Network (2011). Integrated genomic analyses of ovarian carcinoma, *Nature*, 474(7353):609-615.
- CAO, Y., Y. YU, X. CHEN, F. REN, et al. (2018) Low Expression of Protocadherin-8 Promotes the Progression of Ovarian Cancer. *Int J Gynecol Cancer*, 28(2), 346-354.
- CAVALLARO, U. and G. CHRISTOFORI (2004) Cell adhesion and signalling by cadherins and Ig-CAMs in cancer. *Nat Rev Cancer*, 4(2), 118-132.
- CHMELAROVA, M., E. KREPINSKA, J. SPACEK, J. LACO, et al. (2012) Methylation analysis of tumour suppressor genes in ovarian cancer using MS-MLPA. *Folia Biol (Praha)*, 58(6), 246-250.
- CHUNG, Y. W., H. S. BAE, J. Y. SONG, J. K. LEE, et al. (2013) Detection of microRNA as novel biomarkers of epithelial ovarian cancer from the serum of ovarian cancer patients. *Int J Gynecol Cancer*, 23(4), 673-679.
- COTTRELL, S. E., J. DISTLER, N. S. GOODMAN, S. H. MOONEY, et al. (2004) A real-time PCR assay for DNA-methylation using methylation-specific blockers. *Nucleic Acids Res*, 32(1), e10.
- DAVIS, A., A. V. TINKER and M. FRIEDLANDER (2014) "Platinum resistant" ovarian cancer: what is it, who to treat and how to measure benefit? *Gynecol Oncol*, 133(3), 624-631.
- DEJANA, E. Endothelial cell-cell junctions: happy together. (2004) *Nat Rev Mol Cell Biol*, 5(4), 261-270.
- DENG, J., R. SHOEMAKER, B. XIE, A. GORE, et al. (2009) Targeted bisulfite sequencing reveals changes in DNA methylation associated with nuclear reprogramming. *Nat Biotechnol*, 27(4), 353-360.

- DENG, Q. K., Y. G. LEI, Y. L. LIN, J. G. MA, et al. (2016) Prognostic Value of Protocadherin10 (PCDH10) Methylation in Serum of Prostate Cancer Patients. *Med Sci Monit*, 22, 516-521.
- DI LEVA, G., M. GAROFALO and C. M. CROCE (2014) MicroRNAs in cancer. *Annu Rev Pathol*, 9, 287-314.
- DUŠEK, L., J. MUŽÍK, M. KUBÁSEK, J. KOPTÍKOVÁ, et al. (2005) Epidemiologie zhoubných nádorů v České republice [online]. Accessed 2 January 2019. Available at <http://www.svod.cz>.
- EADS, C. A., K. D. DANENBERG, K. KAWAKAMI, L. B. SALTZ, et al. (2000) MethyLight: a high-throughput assay to measure DNA methylation. *Nucleic Acids Res*, 28(8), E32.
- EBRAHIMI, S. O. and S. REIISI (2019) Downregulation of miR-4443 and miR-5195-3p in ovarian cancer tissue contributes to metastasis and tumorigenesis. *Arch Gynecol Obstet*, 10, 4225–4238.
- EHRICH, M., M. R. NELSON, P. STANSSENS, M. ZABEAU, et al. (2005) Quantitative high-throughput analysis of DNA methylation patterns by base-specific cleavage and mass spectrometry. *Proc Natl Acad Sci U S A*, 102(44), 15785-15790.
- ESTECIO, M. R., P. S. YAN, A. E. IBRAHIM, C. S. TELLEZ, et al. (2007) High-throughput methylation profiling by MCA coupled to CpG island microarray. *Genome Res*, 17(10), 1529-1536.
- FANJUL-FERNANDEZ, M., V. QUESADA, R. CABANILLAS, J. CADINANOS, et al. (2013) Cell-cell adhesion genes CTNNA2 and CTNNA3 are tumour suppressors frequently mutated in laryngeal carcinomas. *Nat Commun*, 4, 2531.
- FENG, Q., G. DEFTEREOS, S. E. HAWES, J. E. STERN, et al. (2008) DNA hypermethylation, Her-2/neu overexpression and p53 mutations in ovarian carcinoma. *Gynecol Oncol*, 111(2), 320-329.
- FERLAY, J., M. COLOMBET, I. SOERJOMATARAM, T. DYBA, et al. (2018) Cancer incidence and mortality patterns in Europe: Estimates for 40 countries and 25 major cancers in 2018. *Eur J Cancer*, 103, 356-387.
- FERRACIN, M. and M. NEGRINI (2015) Micromarkers 2.0: an update on the role of microRNAs in cancer diagnosis and prognosis. *Expert Rev Mol Diagn*, 15(10), 1369-1381.
- FISCHEROVÁ, D., M. ZIKÁN, I. PINKAVOVÁ, J. SLÁMA, et al. (2012) Předoperační diagnostika ovariálních nádorů. *Onkologie*, 6(2), 59-64.
- FRIGOLA, J., M. RIBAS, R. A. RISQUES and M. A. PEINADO (2002) Methylome profiling of cancer cells by amplification of inter-methylated sites (AIMS). *Nucleic Acids Res*, 30(7), e28.
- FROMMER, M., L. E. MCDONALD, D. S. MILLAR, C. M. COLLIS, et al. (1992) A genomic sequencing protocol that yields a positive display of 5-methylcytosine residues in individual DNA strands. *Proc Natl Acad Sci U S A*, 89(5), 1827-1831.
- FUKASAWA, M., M. KIMURA, S. MORITA, K. MATSUBARA, et al. (2006) Microarray analysis of promoter methylation in lung cancers. *J Hum Genet*, 51(4), 368-374.
- GONZALGO, M. L. and P. A. JONES (1997) Rapid quantitation of methylation differences at specific sites using methylation-sensitive single nucleotide primer extension (Ms-SNuPE). *Nucleic Acids Res*, 25(12), 2529-2531.

- GONZALGO, M. L., G. LIANG, C. H. SPRUCK 3RD, J. M. ZINGG, et al. (1997) Identification and characterization of differentially methylated regions of genomic DNA by methylation-sensitive arbitrarily primed PCR. *Cancer Res*, 57(4), 594-599.
- GOSPODAROWICZ, M. K., J. D. BRIERLEY and C. WITTEKIND (2017) TNM Classification of Malignant Tumours. Edition ed.: Wiley, 2017. ISBN 9781119263579.
- HARYONO, S. J., I. G. DATASENA, W. B. SANTOSA, R. MULYARAHARDJA, et al. (2015) A pilot genome-wide association study of breast cancer susceptibility loci in Indonesia. *Asian Pac J Cancer Prev*, 16(6), 2231-2235.
- HATADA, I., Y. HAYASHIZAKI, S. HIROTSUNE, H. KOMATSUBARA, et al. (1991) A genomic scanning method for higher organisms using restriction sites as landmarks. *Proc Natl Acad Sci U S A*, 88(21), 9523-9527.
- HATADA, I., A. KATO, S. MORITA, Y. OBATA, et al. (2002) A microarray-based method for detecting methylated loci. *J Hum Genet*, 47(8), 448-451.
- HAUSLER, S. F., A. KELLER, P. A. CHANDRAN, K. ZIEGLER, et al. (2010) Whole blood-derived miRNA profiles as potential new tools for ovarian cancer screening. *Br J Cancer*, 103(5), 693-700.
- HAYASHI, A., A. HORIUCHI, N. KIKUCHI, T. HAYASHI, et al. (2010) Type-specific roles of histone deacetylase (HDAC) overexpression in ovarian carcinoma: HDAC1 enhances cell proliferation and HDAC3 stimulates cell migration with downregulation of E-cadherin. *Int J Cancer*, 127(6), 1332-1346.
- HEIKINHEIMO, K., K. J. JEE, P. R. MORGAN, B. NAGY, et al. (2007) Genetic changes in sporadic keratocystic odontogenic tumors (odontogenic keratocysts). *J Dent Res*, 86(6), 544-549.
- HENTZE, J. L., C. K. HOGDALL and E. V. HOGDALL (2019) Methylation and ovarian cancer: Can DNA methylation be of diagnostic use? *Mol Clin Oncol*, 10(3), 323-330.
- HERMAN, J. G., J. R. GRAFF, S. MYOHANEN, B. D. NELKIN, et al. (1996) Methylation-specific PCR: a novel PCR assay for methylation status of CpG islands. *Proc Natl Acad Sci U S A*, 93(18), 9821-9826.
- HOU, Y. C., J. Y. DENG, R. P. ZHANG, X. M. XIE, et al. (2015) Evaluating the clinical feasibility: The direct bisulfite genomic sequencing for examination of methylated status of protocadherin10 (PCDH10) promoter to predict the prognosis of gastric cancer. *Cancer Biomark*, 15(5), 567-573.
- HUANG, F., J. CHEN, Z. WANG, R. LAN, et al. (2018) delta-Catenin promotes tumorigenesis and metastasis of lung adenocarcinoma. *Oncol Rep*, 39(2), 809-817.
- HUANG, R. L., F. GU, N. B. KIRMA, J. RUAN, et al. (2013) Comprehensive methylome analysis of ovarian tumors reveals hedgehog signaling pathway regulators as prognostic DNA methylation biomarkers. *Epigenetics*, 8(6), 624-634.
- HUANG, T. H., M. R. PERRY and D. E. LAUX (1999) Methylation profiling of CpG islands in human breast cancer cells. *Hum Mol Genet*, 8(3), 459-470.
- HUMPHRIES, J. D., A. BYRON and M. J. HUMPHRIES (2006) Integrin ligands at a glance. *J Cell Sci*, 119(19), 3901-3903.
- IBRAHIM, A. E., N. P. THORNE, K. BAIRD, N. L. BARBOSA-MORAIS, et al. (2006) Mmass: an optimized array-based method for assessing CpG island methylation. *Nucleic Acids Res*, 34(20), e136.

- INTERNATIONAL AGENCY FOR RESEARCH ON CANCER (2019) Global Cancer Observatory: GLOBOCAN 2018 [online]. Accessed 2 January 2019. Available at <http://gco.iarc.fr/>.
- IORIO, M. V., R. VISONE, G. DI LEVA, V. DONATI, et al. (2007) MicroRNA signatures in human ovarian cancer. *Cancer Res*, 67(18), 8699-8707.
- IRIZARRY, R. A., C. LADD-ACOSTA, B. CARVALHO, H. WU, et al. (2008) Comprehensive high-throughput arrays for relative methylation (CHARM). *Genome Res*, 18(5), 780-790.
- JELOVAC, D. and D. K. ARMSTRONG (2011) Recent progress in the diagnosis and treatment of ovarian cancer. *CA Cancer J Clin*, 61(3), 183-203.
- JIN, K. L., J. H. PAK, J. Y. PARK, W. H. CHOI, et al. (2008) Expression profile of histone deacetylases 1, 2 and 3 in ovarian cancer tissues. *J Gynecol Oncol*, 19(3), 185-190.
- JONES, P. A. and S. B. BAYLIN (2002) The fundamental role of epigenetic events in cancer. *Nat Rev Genet*, 3(6), 415-428.
- KAN, C. W., V. M. HOWELL, M. A. HAHN and D. J. MARSH (2015) Genomic alterations as mediators of miRNA dysregulation in ovarian cancer. *Genes Chromosomes Cancer*, 54(1), 1-19.
- KARIMI, M., S. JOHANSSON, D. STACH, M. CORCORAN, et al. (2006) LUMA (LUminometric Methylation Assay) – a high throughput method to the analysis of genomic DNA methylation. *Exp Cell Res*, 312(11), 1989-1995.
- KATZ, B., C. G. TROPE, R. REICH and B. DAVIDSON (2015) MicroRNAs in Ovarian Cancer. *Hum Pathol*, 46(9), 1245-1256.
- KERKEL, K., A. SPADOLA, E. YUAN, J. KOSEK, et al. (2008) Genomic surveys by methylation-sensitive SNP analysis identify sequence-dependent allele-specific DNA methylation. *Nat Genet*, 40(7), 904-908.
- KHULAN, B., R. F. THOMPSON, K. YE, M. J. FAZZARI, et al. (2006) Comparative isoschizomer profiling of cytosine methylation: the HELP assay. *Genome Res*, 16(8), 1046-1055.
- KIM, H., Y. HE, I. YANG, Y. ZENG, et al. (2012) δ -Catenin promotes E-cadherin processing and activates β -catenin-mediated signaling: implications on human prostate cancer progression. *Biochim Biophys Acta*, 1822(4):509-21.
- KIM, M. G., J. H. PAK, W. H. CHOI, J. Y. PARK, et al. (2012) The relationship between cisplatin resistance and histone deacetylase isoform overexpression in epithelial ovarian cancer cell lines. *J Gynecol Oncol*, 23(3), 182-189.
- KOCH, A., S. C. JOOSTEN, Z. FENG, T. C. DE RUIJTER, et al. (2018) Analysis of DNA methylation in cancer: location revisited. *Nat Rev Clin Oncol*, 15(7), 459-466.
- KORESSAAR, T. and M. REMM (2007) Enhancements and modifications of primer design program Primer3. *Bioinformatics*, 23(10), 1289-1291.
- KOUKOURA, O., D. A. SPANDIDOS, A. DAPONTE and S. SIFAKIS (2014) DNA methylation profiles in ovarian cancer: implication in diagnosis and therapy (Review). *Mol Med Rep*, 10(1), 3-9.
- KRISTENSEN, L. S., T. MIKESKA, M. KRYPUY and A. DOBROVIC (2008) Sensitive Melting Analysis after Real Time-Methylation Specific PCR (SMART-MSP): high-throughput and probe-free quantitative DNA methylation detection. *Nucleic Acids Res*, 36(7), e42.

- KURDYUKOV, S. and M. BULLOCK (2016) DNA Methylation Analysis: Choosing the Right Method. *Biology*, 5(1), 3.
- KURMAN, R., CARCANGIU, M. L., HERRINGTON, C. S., and YOUNG, R. H. (2014) WHO Classification of Tumours of Female Reproductive Organs. Fourth Edition IARC Press: Lyon 2014.
- KURMAN, R. J. and M. SHIH IE (2010) The origin and pathogenesis of epithelial ovarian cancer: a proposed unifying theory. *Am J Surg Pathol*, 34(3), 433-443.
- KURMAN, R. J. and M. SHIH IE (2011) Molecular pathogenesis and extraovarian origin of epithelial ovarian cancer – shifting the paradigm. *Hum Pathol*, 42(7), 918-931.
- LAMOUILLE, S., J. XU and R. DERYNCK (2014) Molecular mechanisms of epithelial-mesenchymal transition. *Nat Rev Mol Cell Biol*, 15(3), 178-196.
- LANGHE, R., L. NORRIS, F. A. SAADEH, G. BLACKSHIELDS, et al. (2015) A novel serum microRNA panel to discriminate benign from malignant ovarian disease. *Cancer Lett* 356(2), 628-636.
- LEE, J. Y. and G. KONG (2016) Roles and epigenetic regulation of epithelial-mesenchymal transition and its transcription factors in cancer initiation and progression. *Cell Mol Life Sci*, 73(24), 4643-4660.
- LEE, Y., A. MIRON, R. DRAPKIN, M. R. NUCCI, et al. (2007) A candidate precursor to serous carcinoma that originates in the distal fallopian tube. *J Pathol*, 211(1), 26-35.
- LEY, K. (2003) The role of selectins in inflammation and disease. *Trends Mol Med*, 9(6), 263-268.
- LI, C., Z. GAO, F. LI, X. LI, et al. (2015) Whole Exome Sequencing Identifies Frequent Somatic Mutations in Cell-Cell Adhesion Genes in Chinese Patients with Lung Squamous Cell Carcinoma. *Sci Rep*, 5, 14237.
- LI, L. C. and R. DAHIYA (2002) MethPrimer: designing primers for methylation PCRs. *Bioinformatics*, 18(11), 1427-1431.
- LI, Y., C. LIU, Z. WANG and G. HU (2018) Expression of protocadherin8: Function as a tumor suppressor in hypopharyngeal carcinoma. *Cancer Biomark*, 22(3), 495-502.
- LIN, Y. L., S. L. GUI and J. G. MA (2015) Aberrant methylation of CDH11 predicts a poor outcome for patients with bladder cancer. *Oncol Lett*, 10(2), 647-652.
- LIN, Y. L., Y. L. WANG, J. G. MA and W. P. LI (2014) Clinical significance of protocadherin 8 (PCDH8) promoter methylation in non-muscle invasive bladder cancer. *J Exp Clin Cancer Res*, 33, 68.
- LISTER, R., M. PELIZZOLA, R. H. DOWEN, R. D. HAWKINS, et al. (2009) Human DNA methylomes at base resolution show widespread epigenomic differences. *Nature*, 462(7271), 315-322.
- LUO, Z. G., Z. G. LI, S. L. GUI, B. J. CHI, et al. (2014) Protocadherin-17 promoter methylation in serum-derived DNA is associated with poor prognosis of bladder cancer. *J Int Med Res*, 42(1), 35-41.
- MANCHANDA, R., R. LEGOOD, M. BURNELL, A. MCGUIRE, et al. (2015) Cost-effectiveness of population screening for BRCA mutations in Ashkenazi jewish women compared with family history-based testing. *J Natl Cancer Inst*, 107(1), 380.
- MATEI, D., F. FANG, C. SHEN, J. SCHILDER, et al. (2012) Epigenetic resensitization to platinum in ovarian cancer. *Cancer Res*, 72(9), 2197-2205.

- MEISSNER, A., A. GNIRKE, G. W. BELL, B. RAMSAHOYE, et al. (2005) Reduced representation bisulfite sequencing for comparative high-resolution DNA methylation analysis. *Nucleic Acids Res*, 33(18), 5868-5877.
- MERKEL, A., M. FERNANDEZ-CALLEJO, E. CASALS, S. MARCO-SOLA, et al. (2019) gemBS: high throughput processing for DNA methylation data from bisulfite sequencing. *Bioinformatics*, 35(5), 737-742.
- MONTAVON, C., B. S. GLOSS, K. WARTON, C. A. BARTON, et al. (2012) Prognostic and diagnostic significance of DNA methylation patterns in high grade serous ovarian cancer. *Gynecol Oncol*, 124(3), 582-588.
- MOORE, R. G., D. S. MCMEEKIN, A. K. BROWN, P. DISILVESTRO, et al. (2009) A novel multiple marker bioassay utilizing HE4 and CA125 for the prediction of ovarian cancer in patients with a pelvic mass. *Gynecol Oncol*, 112(1), 40-46.
- MORISHITA, H. and T. YAGI (2007) Protocadherin family: diversity, structure, and function. *Curr Opin Cell Biol*, 19(5), 584-592.
- MOSCHETTA, M., A. GEORGE, S. B. KAYE and S. BANERJEE (2016) BRCA somatic mutations and epigenetic BRCA modifications in serous ovarian cancer. *Ann Oncol*, 27(8), 1449-1455.
- MOUFARRIJ, S., M. DANDAPANI, E. ARTHOFER, S. GOMEZ, et al. (2019) Epigenetic therapy for ovarian cancer: promise and progress. *Clin Epigenetics*, 11(1), 7.
- NAM, E. J., H. YOON, S. W. KIM, H. KIM, et al. (2008) MicroRNA expression profiles in serous ovarian carcinoma. *Clin Cancer Res*, 14(9), 2690-2695.
- NIU, W.-B., S.-L. GUI, Y.-L. LIN, X.-L. FU, et al. (2014) Promoter Methylation of Protocadherin8 is an Independent Prognostic Factor for Biochemical Recurrence of Early-Stage Prostate Cancer. *Med Sci Monit*, 20, 2584-2589.
- NYGREN, A. O., N. AMEZIANE, H. M. DUARTE, R. N. VIJZELAAR, et al. (2005) Methylation-specific MLPA (MS-MLPA): simultaneous detection of CpG methylation and copy number changes of up to 40 sequences. *Nucleic Acids Res*, 33(14), e128.
- ODA, M., J. L. GLASS, R. F. THOMPSON, Y. MO, et al. (2009) High-resolution genome-wide cytosine methylation profiling with simultaneous copy number analysis and optimization for limited cell numbers. *Nucleic Acids Res*, 37(12), 3829-3839.
- OKEGAWA, T., R. C. PONG, Y. LI and J. T. HSIEH (2004) The role of cell adhesion molecule in cancer progression and its application in cancer therapy. *Acta Biochim Pol*, 51(2), 445-457.
- OLKHOV-MITSEL, E. and B. BAPAT (2012) Strategies for discovery and validation of methylated and hydroxymethylated DNA biomarkers. *Cancer Med*, 1(2), 237-260.
- ORDWAY, J. M., J. A. BEDELL, R. W. CITEK, A. NUNBERG, et al. (2006) Comprehensive DNA methylation profiling in a human cancer genome identifies novel epigenetic targets. *Carcinogenesis*, 27(12), 2409-2423.
- PDQ® Adult Treatment Editorial Board. PDQ Ovarian Epithelial, Fallopian Tube, and Primary Peritoneal Cancer Treatment. Bethesda, MD: National Cancer Institute. Updated 1 February 2019, accessed 6 March 2019. Available at <https://www.cancer.gov/types/ovarian/hp/ovarian-epithelial-treatment-pdq>.

- PRAT, J. (2012) Ovarian carcinomas: five distinct diseases with different origins, genetic alterations, and clinicopathological features. *Virchows Arch*, 460(3), 237-249.
- RATHI, A., A. K. VIRMANI, J. O. SCHORGE, K. J. ELIAS, et al. (2002) Methylation profiles of sporadic ovarian tumors and nonmalignant ovaries from high-risk women. *Clin Cancer Res*, 8(11), 3324-3331.
- RAUCH, T. and G. P. PFEIFER (2005) Methylated-CpG island recovery assay: a new technique for the rapid detection of methylated-CpG islands in cancer. *Lab Invest*, 85(9), 1172-1180.
- REINDERS, J., C. DELUCINGE VIVIER, G. THEILER, D. CHOLLET, et al. (2008) Genome-wide, high-resolution DNA methylation profiling using bisulfite-mediated cytosine conversion. *Genome Res*, 18(3), 469-476.
- RESNICK, K. E., H. ALDER, J. P. HAGAN, D. L. RICHARDSON, et al. (2009) The detection of differentially expressed microRNAs from the serum of ovarian cancer patients using a novel real-time PCR platform. *Gynecol Oncol*, 112(1), 55-59.
- ROBINSON, J. T., H. THORVALDSDÓTTIR, W. WINCKLER, M. GUTTMAN, et al. (2011) Integrative genomics viewer. *Nature biotechnology*, 29(1), 24-26.
- SELVAKUMARAN, M., D. A. PISARCIK, R. BAO, A. T. YEUNG, et al. (2003) Enhanced cisplatin cytotoxicity by disturbing the nucleotide excision repair pathway in ovarian cancer cell lines. *Cancer Res*, 63(6), 1311-1316.
- SHAHAB, S. W., L. V. MATYUNINA, C. G. HILL, L. WANG, et al. (2012) The effects of MicroRNA transfections on global patterns of gene expression in ovarian cancer cells are functionally coordinated. *BMC Med Genomics*, 5, 33.
- SHAN, M., Y. SU, W. KANG, R. GAO, et al. (2016) Aberrant expression and functions of protocadherins in human malignant tumors. *Tumour Biol*, 37(10), 12969-12981.
- SHAPIRA, I., M. OSWALD, J. LOVECCHIO, H. KHALILI, et al. (2014) Circulating biomarkers for detection of ovarian cancer and predicting cancer outcomes. *Br J Cancer*, 110(4), 976-983.
- SHIH IE, M. and R. J. KURMAN (2004) Ovarian tumorigenesis: a proposed model based on morphological and molecular genetic analysis. *Am J Pathol*, 164(5), 1511-1518.
- SMITH, H. J., J. M. STRAUGHN, D. J. BUCHSBAUM and R. C. AREND (2017) Epigenetic therapy for the treatment of epithelial ovarian cancer: A clinical review. *Gynecol Oncol Rep*, 20, 81-86.
- SORRENTINO, A., C. G. LIU, A. ADDARIO, C. PESCHLE, et al. (2008) Role of microRNAs in drug-resistant ovarian cancer cells. *Gynecol Oncol*, 111(3), 478-486.
- STELZER, G., R. ROSEN, I. PLASCHKES, S. ZIMMERMAN, et al. (2016) The GeneCards Suite: From Gene Data Mining to Disease Genome Sequence Analysis. *Current Protocols in Bioinformatics*, 54:1.30.1-1.30.33. Updated 31 January 2019, accessed 26 April 2019. Available at www.genecards.org.
- STRATHDEE, G. (2002) Epigenetic versus genetic alterations in the inactivation of E-cadherin. *Semin Cancer Biol*, 12(5), 373-379.
- STUART, G. C., H. KITCHENER, M. BACON, A. DUBOIS, et al. (2011) 2010 Gynecologic Cancer InterGroup (GCIg) consensus statement on clinical trials in ovarian cancer: report from the Fourth Ovarian Cancer Consensus Conference. *Int J Gynecol Cancer*, 21(4), 750-755.

- TAKADA, Y., X. YE and S. SIMON (2007) The integrins. *Genome Biol*, 8(5), 215.
- TANG, X., X. YIN, T. XIANG, H. LI, et al. (2012) Protocadherin 10 is frequently downregulated by promoter methylation and functions as a tumor suppressor gene in non-small cell lung cancer. *Cancer Biomark*, 12(1), 11-19.
- THIERY, J. P., H. ACLOQUE, R. Y. HUANG and M. A. NIETO (2009) Epithelial-mesenchymal transitions in development and disease. *Cell*, 139(5), 871-890.
- TODESCHINI, P., E. SALVIATO, L. PARACCHINI, M. FERRACIN, et al. (2017) Circulating miRNA landscape identifies miR-1246 as promising diagnostic biomarker in high-grade serous ovarian carcinoma: A validation across two independent cohorts. *Cancer Lett*, 388, 320-327.
- TOYOTA, M., C. HO, N. AHUJA, K. W. JAIR, et al. (1999) Identification of differentially methylated sequences in colorectal cancer by methylated CpG island amplification. *Cancer Res*, 59(10), 2307-2312.
- UNTERGASSER, A., I. CUTCUTACHE, T. KORESSAAR, J. YE, et al. (2012) Primer3- new capabilities and interfaces. *Nucleic Acids Res*, 40(15), e115.
- VAN VLODROP, I. J., H. E. NIESSEN, S. DERKS, M. M. BALDEWIJNS, et al. (2001) Analysis of promoter CpG island hypermethylation in cancer: location, location, location! *Clin Cancer Res*, 17(13), 4225-4231.
- VAN ZYL, B., D. TANG and N. A. BOWDEN (2018) Biomarkers of platinum resistance in ovarian cancer: what can we use to improve treatment. *Endocr Relat Cancer*, 25(5), R303-R318.
- VANG, R., M. SHIH IE and R. J. KURMAN (2013) Fallopian tube precursors of ovarian low- and high-grade serous neoplasms. *Histopathology*, 62(1), 44-58.
- VANG, R., I.-M. SHIH and R. J. KURMAN (2009) Ovarian low-grade and high-grade serous carcinoma: Pathogenesis, Clinicopathologic and Molecular Biologic Features, and Diagnostic Problems. *Adv Anat Pathol*, 16(5), 267-282.
- VENKATACHALAM, R., E. T. VERWIEL, E. J. KAMPING, E. HOENSELAAR, et al. (2011) Identification of candidate predisposing copy number variants in familial and early-onset colorectal cancer patients. *Int J Cancer*, 129(7), 1635-1642.
- VERGARA, D., B. MERLOT, J. P. LUCOT, P. COLLINET, et al. (2010) Epithelial-mesenchymal transition in ovarian cancer. *Cancer Lett*, 291(1), 59-66.
- VILMING ELGAAEN, B., O. K. OLSTAD, K. B. HAUG, B. BRUSLETTO, et al. (2014) Global miRNA expression analysis of serous and clear cell ovarian carcinomas identifies differentially expressed miRNAs including miR-200c-3p as a prognostic marker. *BMC Cancer*, 14, 80.
- WAI WONG, C., D. E. DYE and D. R. COOMBE (2012) The role of immunoglobulin superfamily cell adhesion molecules in cancer metastasis. *Int J Cell Biol*, 340296.
- WALKER, M. M., S. M. ELLIS, M. J. AUZA, A. PATEL, et al. (2008) The intercellular adhesion molecule, cadherin-10, is a marker for human prostate luminal epithelial cells that is not expressed in prostate cancer. *Mod Pathol*, 21(2), 85-95.
- WANG, Q., B. WANG, Y. M. ZHANG and W. WANG (2016) The association between CDH1 promoter methylation and patients with ovarian cancer: a systematic meta-analysis. *J Ovarian Res*, 9, 23.

- WEBER, M., J. J. DAVIES, D. WITTIG, E. J. OAKELEY, et al. (2005) Chromosome-wide and promoter-specific analyses identify sites of differential DNA methylation in normal and transformed human cells. *Nat Genet*, 37(8), 853-862.
- WEIDERPASS, E. and J. E. TYCZYNSKI (2015) Epidemiology of Patients with Ovarian Cancer with and Without a BRCA1/2 Mutation. *Mol Diagn Ther*, 19(6), 351-364.
- WEICHERT, W., C. DENKERT, A. NOSKE, S. DARB-ESFAHANI, et al. (2008) Expression of class I histone deacetylases indicates poor prognosis in endometrioid subtypes of ovarian and endometrial carcinomas. *Neoplasia*, 10(9), 1021-1027.
- WOJDACZ, T. K. and A. DOBROVIC (2007) Methylation-sensitive high resolution melting (MS-HRM): a new approach for sensitive and high-throughput assessment of methylation. *Nucleic Acids Res*, 35(6), e41.
- WORM, J., A. AGGERHOLM and P. GULDBERG (2001) In-tube DNA methylation profiling by fluorescence melting curve analysis. *Clin Chem*, 2001, 47(7), 1183-1189.
- WU, X., Y. X. ZHUANG, C. Q. HONG, J. Y. CHEN, et al. (2014) Clinical importance and therapeutic implication of E-cadherin gene methylation in human ovarian cancer. *Med Oncol*, 31(8), 100.
- WYMAN, S. K., R. K. PARKIN, P. S. MITCHELL, B. R. FRITZ, et al. (2009) Repertoire of microRNAs in epithelial ovarian cancer as determined by next generation sequencing of small RNA cDNA libraries. *PLoS One*, 4(4), e5311.
- XIONG, Z. and P. W. LAIRD (1997) COBRA: a sensitive and quantitative DNA methylation assay. *Nucleic Acids Res*, 25(12), 2532-2534.
- YEGNASUBRAMANIAN, S., X. LIN, M. C. HAFFNER, A. M. DEMARZO, et al. (2006) Combination of methylated-DNA precipitation and methylation-sensitive restriction enzymes (COMPARE-MS) for the rapid, sensitive and quantitative detection of DNA methylation. *Nucleic Acids Res*, 34(3), e19.
- YIN, X., T. XIANG, J. MU, H. MAO, et al. (2016) Protocadherin 17 functions as a tumor suppressor suppressing Wnt/ β -catenin signaling and cell metastasis and is frequently methylated in breast cancer. *Oncotarget*, 7(32), 51720-51732.
- ZAVESKY, L., E. JANDAKOVA, R. TURZYNA, L. LANGMEIEROVA, et al. (2015) Evaluation of Cell-Free Urine microRNAs Expression for the Use in Diagnosis of Ovarian and Endometrial Cancers. A Pilot Study. *Pathol Oncol Res*, 21(4), 1027-1035.
- ZEPPERINICK, F., I. MEINHOLD-HEERLEIN and I.-M. SHIH (2015) Precursors of ovarian cancer in the fallopian tube: Serous tubal intraepithelial carcinoma – an update. *J Obstet Gynaecol Res*, 41(1), 6-11.
- ZHANG, Q., J. E. BURDETTE and J.-P. WANG (2014) Integrative network analysis of TCGA data for ovarian cancer. *BMC Systems Biology*, 8(1), 1-18.
- ZHENG, H., L. ZHANG, Y. ZHAO, D. YANG, et al. (2013) Plasma miRNAs as diagnostic and prognostic biomarkers for ovarian cancer. *PLoS One*, 8(11), e77853.

Appendices

A1 FIGO staging classification for cancer of the ovary, fallopian tube, and peritoneum

Table A1.1 FIGO staging classification for cancer of the ovary, fallopian tube, and peritoneum

TNM categories	FIGO stage	Definition	
TX		Primary tumor cannot be assessed	
T0		No evidence of primary tumor	
T1	I	Tumor limited to the ovaries (one or both) or FT(s)	
T1a	IA	Tumor limited to one ovary; capsule intact, no tumor on ovarian surface or FT surface; no malignant cells in ascites or peritoneal washings	
T1b	IB	Tumor limited to both ovaries or FTs; capsule intact, no tumor on ovarian or FT surface; no malignant cells in ascites or peritoneal washings	
T1c	IC	Tumor limited to one or both ovaries or FTs with any of the following:	
T1c1		surgical spill	
T1c2		capsule ruptured before surgery or tumor on ovarian or FT surface	
T1c3		malignant cells in ascites or peritoneal washings	
T2	II	Tumor involves one or both ovaries or FTs with pelvic extension (below the pelvic brim) or primary peritoneal cancer	
T2a	IIA	Extension and/or implants on uterus and/or FT(s) and or ovary(ies)	
T2b	IIB	Extension to other pelvic tissues, including bowel within the pelvis	
T3	III	Tumor involves one or both ovaries or FTs or primary peritoneal carcinoma with cytologically or histologically confirmed spread to the peritoneum outside the pelvis and/or metastasis to the retroperitoneal lymph nodes	
N1	N1a	III A1i	Lymph node metastasis not more than 10 mm in greatest dimension
	N1b	III A1ii	Lymph node metastasis more than 10 mm in greatest dimension
T3a any N		III A2	Microscopic extrapelvic (above the pelvic brim) peritoneal involvement with or without retroperitoneal lymph node, including bowel involvement
T3b any N		III B	Macroscopic peritoneal metastasis beyond pelvic brim 2 cm, or less in greatest dimension, including bowel involvement outside the pelvis with or without retroperitoneal nodes
T3c any N		III C	Peritoneal metastasis beyond pelvic brim more than 2 cm in greatest dimension and/or retroperitoneal lymph node metastasis (includes extension of tumor to capsule of liver and spleen without parenchymal involvement of either organ)
M1		IV	Distant metastasis (excludes peritoneal metastasis)
M1a			Pleural effusion with positive cytology
M1b			Parenchymal metastasis and metastasis to extra abdominal organs (including inguinal lymph nodes and lymph nodes outside the abdominal cavity)

FT, fallopian tube

A2 Methylation of catenins detected by next-generation sequencing

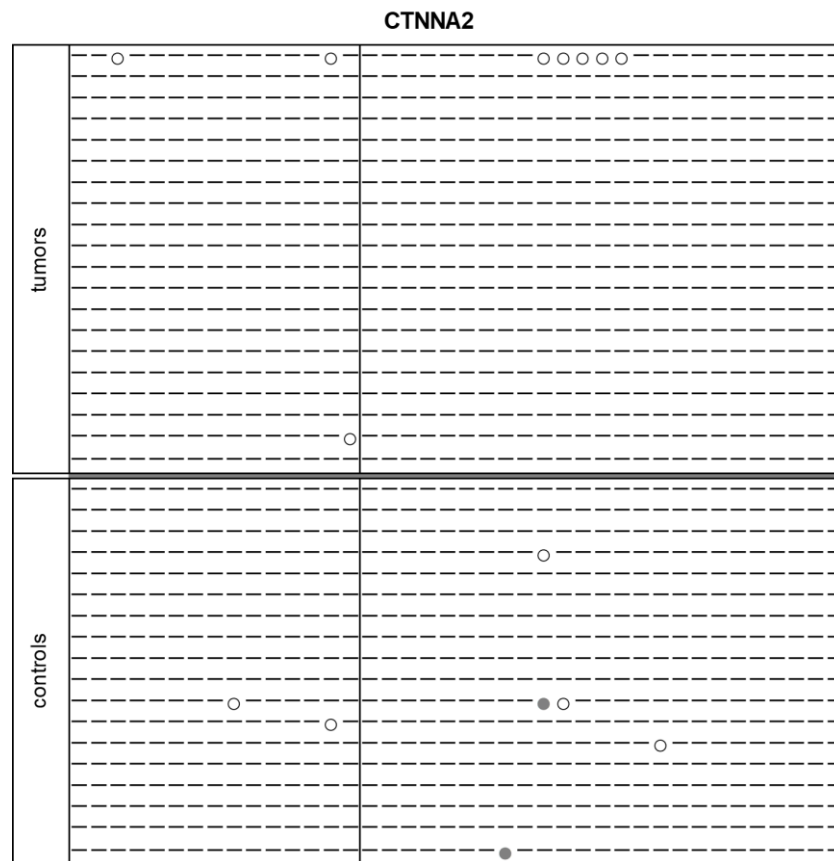


Figure A2.1 Next-generation sequencing methylation data of *CTNNA2*. Each dash represents CpG without methylation (cut-off 15%). Methylated CpGs are displayed as circles: white 15–24.9% and grey 25–49.9% methylation. Grey band in the middle of the table marks CpGs clustered in CpG island.

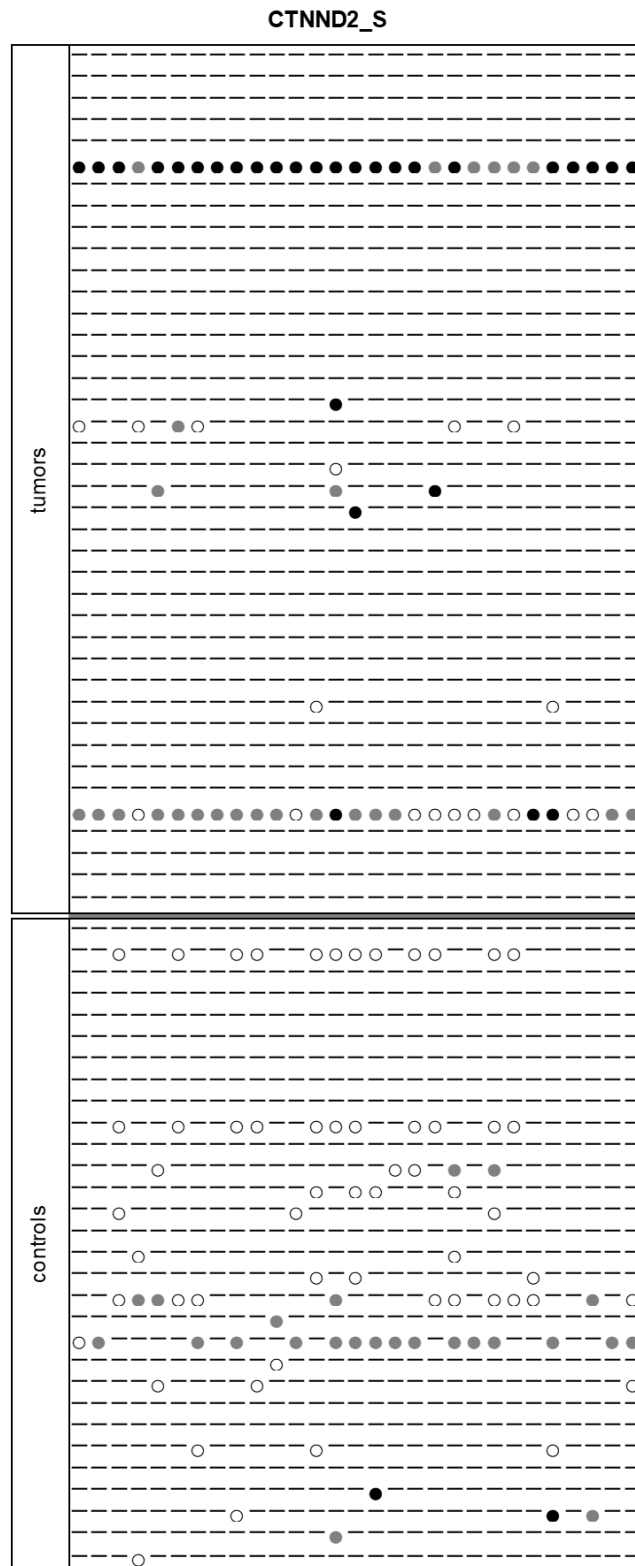


Figure A2.2 Next-generation sequencing methylation data of *CTNND2*, short amplicon. Each dash represents CpG without methylation (cut-off 15%). Methylated CpGs are displayed as circles: white 15–24.9%, grey 25–49.9% and black over 50% methylation. Grey band in the middle of the table marks CpGs clustered in CpG island.

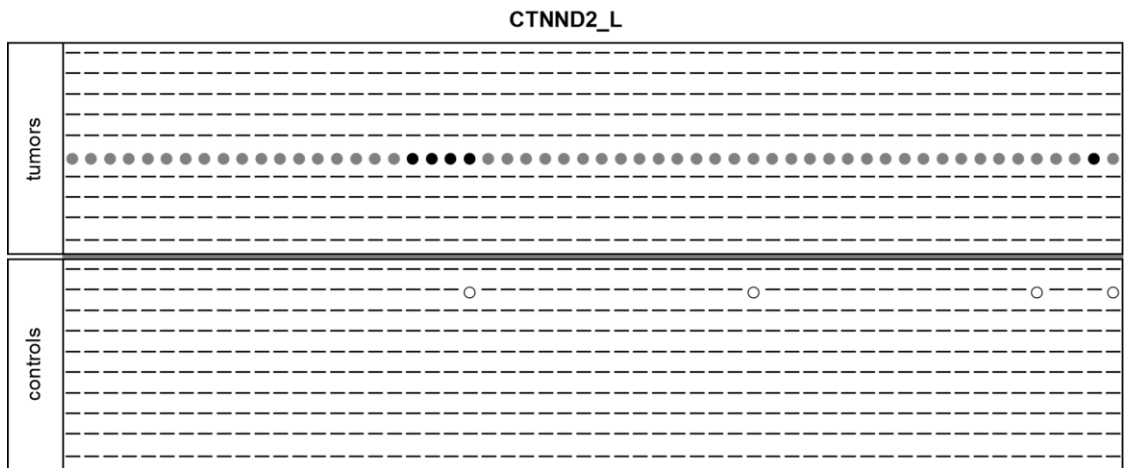


Figure A2.3 Next-generation sequencing methylation data of *CTNND2*, long amplicon. Each dash represents CpG without methylation (cut-off 15%). Methylated CpGs are displayed as circles: white 15–24.9%, grey 25–49.9% and black over 50% methylation. Grey band in the middle of the table marks CpGs clustered in CpG island.

A3 Follow-up data of patients and methylation status of analyzed genes

Table A3.1 Follow-up data of patients and methylation status of analyzed genes

No.	Status 1/2019	OS (months)	Relapse	DFS (months)	Comment	Methylation			
						CDH13	PCDH17	GATA4	HNF1B
1	dead	37	yes	14		M	M	M	M
2	dead	44	no	-		U	M	M	M
3	dead	2	no	-		U	M	M	U
4	dead	57	yes	12		M	M	U	M
5	n/a	n/a	yes	43		U	U	U	U
6	alive	139*	no	132*	remission	U	U	U	M
7	dead	24	no	-		M	M	M	M
8	dead	70	-	0	progression	U	M	U	U
9	n/a	n/a	yes	62		U	M	M	U
10	dead	28	yes	8		U	M	U	U
11	dead	14	-	0	persistence	U	M	U	U
12	dead	63	yes	20		U	M	M	U
13	dead	114	yes	81		U	M	U	U
14	dead	40	yes	29		U	U	U	M
15	dead	96	yes	35		U	U	U	U
16	n/a	n/a	no	-	remission of C56, C50 duplicity	M	U	U	U
17	dead	63	yes	9		U	M	U	U
18	dead	24	-	0	persistence	U	U	U	U
19	n/a	n/a	n/a	n/a		U	M	U	U
20	dead	10	-	0	persistence	U	M	M	M
21	alive	181*	no	172*	remission	M	M	M	M
22	dead	28	yes	7		U	U	U	U
23	dead	79	yes	18		M	M	U	U
24	dead	124	yes	32		U	M	U	M
25	dead	24	-	0	persistence	U	M	U	U
26	dead	47	yes	18		U	M	M	M
27	dead	28	-	0	persistence	U	U	U	U
28	dead	142	yes	52		U	U	U	M
29	dead	46	yes	22		U	M	U	M
30	dead	65	yes	16		U	U	U	M
31	alive	148*	no	97*	remission	U	U	U	U
32	alive	216*	no	211*	remission	U	M	U	U
33	n/a	n/a	n/a	n/a		U	M	M	U
34	alive	118*	yes	71		U	U	M	U
35	alive	160*	no	154*	remission	U	M	U	M
36	alive	174*	no	169*	remission	U	U	M	U
37	dead	53	yes	6		M	M	U	M
38	alive	85*	yes	19	C50 duplicity	U	M	M	U
39	dead	65	yes	15		U	U	U	M
40	alive	54*	no	49*	remission	U	M	U	M
41	alive	51*	no	45*	remission	M	M	M	U
42	n/a	n/a	n/a	n/a		U	M	M	M

No.	Status 1/2019	OS (months)	Relapse	DFS (months)	Comment	Methylation			
						CDH13	PCDH17	GATA4	HNF1B
43	n/a	n/a	yes	10		U	U	U	M
44	alive	45*	no	39*	remission	U	M	M	M
45	n/a	n/a	yes	8		U	M	U	M
46	n/a	n/a	-	0	progression	U	U	U	M
47	alive	41*	no	36*	remission	U	U	U	M
48	alive	41*	yes	7		M	M	U	M
49	n/a	n/a	n/a	n/a		U	U	U	M
50	alive	40*	no	34*	remission	U	M	U	U
51	dead	12	-	0	progression	M	U	U	U
52	n/a	n/a	-	0	progression	U	M	U	M
53	alive	60*	yes	41		M	M	U	M
54	n/a	n/a	-	0	progression	U	U	M	U
55	alive	35*	yes	15		U	M	M	M
56	n/a	n/a	-	0	progression	U	M	M	U
57	alive	21*	no	8*		U	U	U	M
58	alive	21*	no	8*		U	U	U	U
59	n/a	n/a	n/a	n/a		M	U	U	U
60	n/a	n/a	yes	22		U	U	U	M
61	alive	71*	no	64*	remission of C56, C50 duplicity	U	M	U	M

* marks unfinished time period. OS, overall survival; DFS, disease-free survival; n/a, data not available; C56, ovarian cancer; C50, breast cancer; M, methylated; U, unmethylated.

A4 Methylation analysis of *HNF1B* and *GATA4* genes

Next-generation sequencing

NGS was performed on Illumina MiSeq® System following the same procedure as described in methods part, paragraph 3.4. Next-generation sequencing. Genomic coordinates, primer sequences and amplicons' information are listed in Table A4.1. First PCRs were conducted in the Veriti™ Thermal Cycler (Thermo Fisher Scientific) following the protocol in Table 5 according to PCR thermal profile II at annealing temperature 60 °C. The schematic representation of detected methylation is shown in Figure A4.1.

Table A4.1 Amplicon characteristics and primer sequences used for next-generation sequencing of *GATA4* and *HNF1B*

Amplicon name	<i>GATA4</i>	<i>HNF1B</i>
Coordinates	hg38_chr8:11,704,048-11,704,310 (+)	hg38_chr17:37,745,277-37,745,633 (-)
CpGs / Amplicon ^s (bp)	28 / 271	19 / 357
Primer sequence 5'-3'	Fw: *GATTTTGTGGTTGGGGGAG Rv: *CCCTACCTACTAACCTAAAAATTCC	Fw: *AAATAAATGGAGTTTTTTAGGGTATGT Rv: *AATTCTACTTATCAACCAAACCTCACC

^s amplicon size without adapters and barcodes

* adapter overhangs: Fw: AAGACTCGGCAGCATCTCCA, Rv: GCGATCGTCACTGTTCTCCA

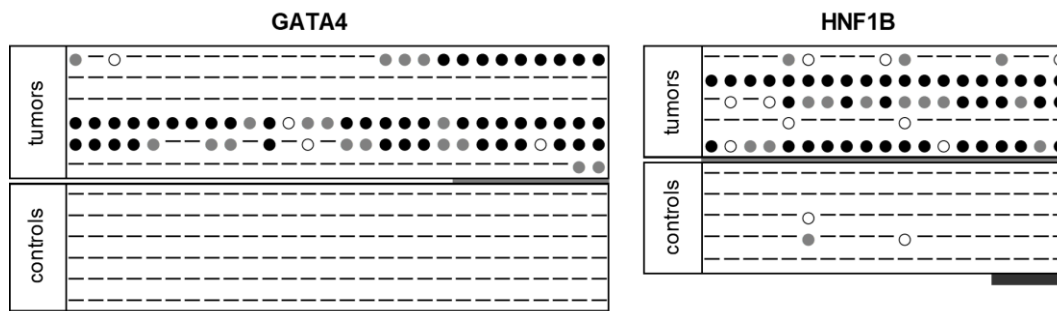


Figure A4.1 Next-generation sequencing methylation data of *GATA4* and *HNF1B*. Each dash represents CpG without methylation (cut-off 15%). Methylated CpGs are displayed as circles: white 15–24.9%, grey 25–49.9% and black over 50% methylation. Grey band in the middle of each table marks CpGs clustered in CpG island. Black band at the bottom of the table with *GATA4* methylation data shows the gene region covered by real-time PCR assay. Black band at the bottom of the table with *HNF1B* methylation data shows the gene region covered by HRM assay.

Real-time methylation specific analysis of GATA4 gene

To confirm the presence of methylation detected by NGS, 4 CpGs (Figure A4.1) were selected for further analysis using real-time methylation specific analysis. PCRs were performed on the Rotor-Gene Q (Qiagen) in two types of reaction mixture within one run; one mixture for amplifying methylated DNA, and the second one for amplifying unmethylated DNA. Primer sequences for methylated DNA were as follows: forward primer 5'-GTTTCGTCGTCGTTGTAGTTTC-3', reverse primer 5'-ATAAAATAAATAACGCACGTCTCTT-3', with amplicon length 197 bp. Primer sequences for unmethylated DNA: 5'-TTTGTTGTTGTTGTAGTTTTGGG-3' and 5'-TAAAATAAATAACACACATCTCTT-3', with amplicon length 194 bp. As fluorochrome dsDNA binding dye SYTO9 was used. PCRs were conducted according to the protocol in Table A4.2. Each run included a bisulfite-converted universal methylated and unmethylated DNA (Qiagen) and the no template control.

Table A4.2 PCR protocol for methylation specific analysis of *GATA4*

PCR setup		
Component		Volume
RNase-free water		to 20 μ L
10X Reaction Buffer no MgCl ₂		2 μ L
MgCl ₂ (25 mM)		2 μ L
dNTP Mix (2.5 mM)		1.6 μ L
Forward primer M/U* (10 μ M)		0.5 μ L
Reverse primer M/U* (10 μ M)		0.5 μ L
SYTO 9 dye		0.3 μ L
AmpliTaq Gold DNA Polymerase (5 U/ μ L)		0.25 μ L
Template DNA		1.5 μ L
PCR thermal profile		
Step	Temperature ($^{\circ}$ C)	
Initial denaturation	95	5 minutes
40 PCR Cycles	Denature	95
	Anneal	58
	Extend	72
Hold	40	2 minutes

* Two reaction mixtures: one with set of methylated (M) primers, the second one with unmethylated (U) primers

Fluorescence data were analyzed using Rotor-Gene Q software. The methylation status of amplicon was determined by calculating methylation index:

$$MI (\%) = 100 / (1 + 2^{(CT_m - CT_u)})$$

CT_m represents Ct value of the reaction with primer pair for methylated DNA; CT_u is Ct value of the reaction with primer pair for unmethylated DNA. For amplicon to be considered methylated the value of MI had to be over 5 %. Where there was reaction only in the reaction mixture with primer pair for unmethylated DNA, the amplicon was considered unmethylated.

Statistically significant methylation ($p < 0.01$) was detected in 31.2 % (19/61) of tumor samples. All control samples were methylation free. Methylation was detected with the similar frequency in the early stage (28.6 %, 4/14) and late stage tumors (31.9 %, 15/47).

High-resolution melting analysis of HNF1B gene

Based on the results from NGS, primers for MS-HRM analysis were designed for confirmation of detected *HNF1B* hypermethylation. Selected region covered 4 CpGs (Figure A4.1).

MS-HRM analysis of *HNF1B* followed the same procedure as described in methods part, paragraph 3.5.1. Methylation sensitive high-resolution melting analysis. Sequence of forward primer was 5'-TTTTGGATTAAAGYGGAATTGAG-3'; sequence of reverse primer 5'-TCCATTATACTCACRCTAAAAAAC-3', with amplicon length 153 bp. Amplicon included 5 CpG sites. PCR amplification and MS-HRM analysis were conducted according to the protocol in Table A4.3.

Statistically significant methylation-positive pattern ($p < 0.01$) was observed in 50.8 % (31/61) of the tumor samples. There was no detected methylation in any of the control samples. In the late stage tumors, methylation was detected in 57.5 % (27/47) of cases, versus 28.6 % (4/14) of the early stage tumors. However, the difference was statistically considered just borderline significant ($p = 0.07$).

Table A4.3 Protocol for MS-HRM analysis of *HNFI1B*

PCR setup		
Component		Volume
RNase-free water		to 20 μ L
10X Reaction Buffer no MgCl ₂		2 μ L
MgCl ₂ (25 mM)		2 μ L
dNTP Mix (2.5 mM)		1.6 μ L
Forward primer (10 μ M)		0.5 μ L
Reverse primer (10 μ M)		0.5 μ L
SYTO 9 dye		0.3 μ L
AmpliTaq Gold DNA Polymerase (5 U/ μ L)		0.25 μ L
Template DNA		2 μ L
PCR thermal profile		
Step	Temperature ($^{\circ}$ C)	Time
Initial denaturation	95	5 minutes
45 PCR Cycles	Denature	95
	Anneal	60
	Extend	72
Final Extension	72	5 minutes
HRM	65-85; Δ 0.1	2 seconds
Hold	40	2 minutes